Journal of Materials Chemistry

www.rsc.org/materials

Volume 21 | Number 45 | 7 December 2011 | Pages 18097–18476

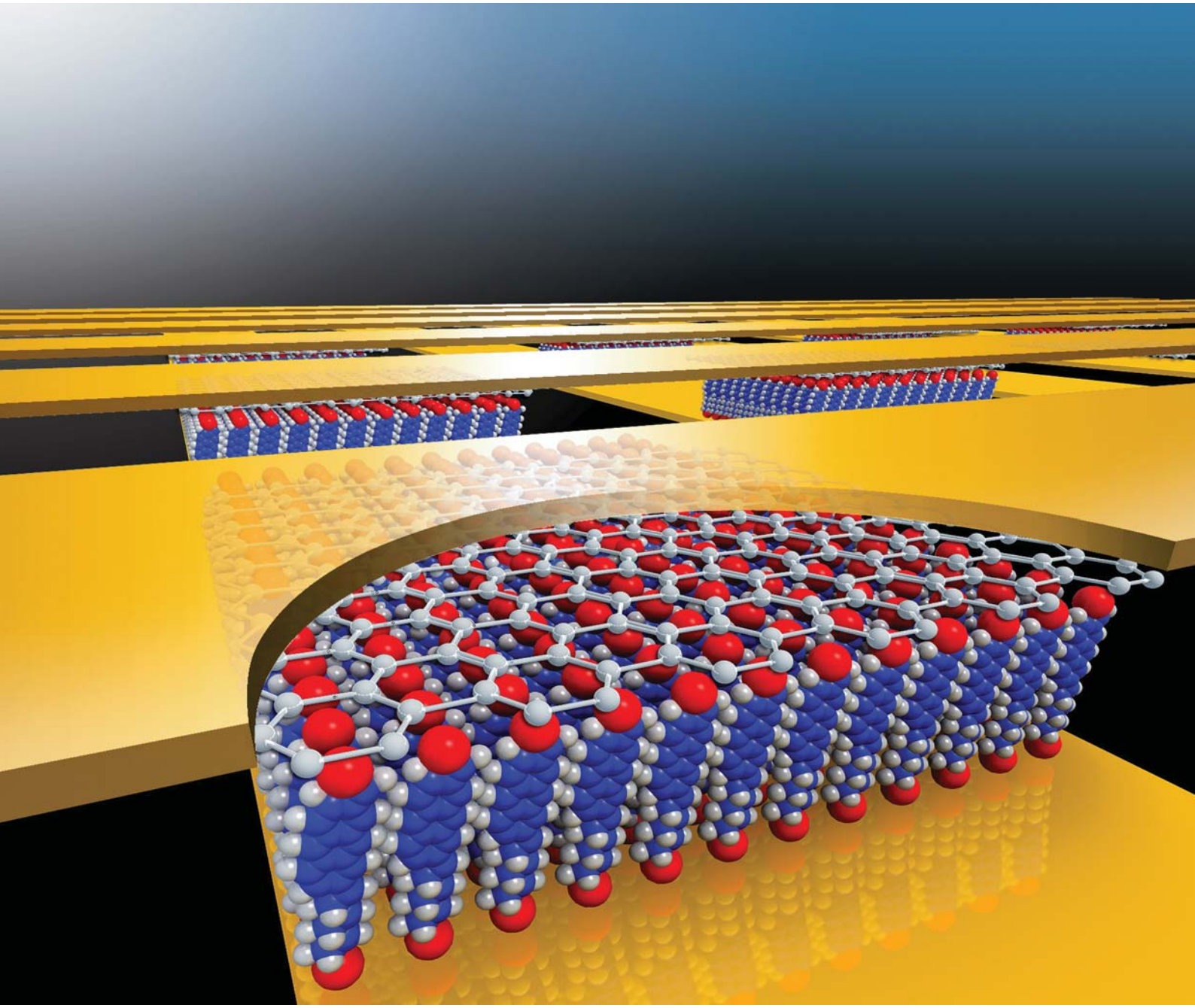

ISSN 0959-9428

RSC Publishing

FEATURE ARTICLE

Takhee Lee *et al.*

Electrical transport characteristics through molecular layers

International Year of CHEMISTRY 2011

0959-9428(2011)21:45;1-C

Journal of Materials Chemistry

Dynamic Article Links

Cite this: *J. Mater. Chem.*, 2011, **21**, 18117

www.rsc.org/materials

FEATURE ARTICLE

Electrical transport characteristics through molecular layers

Gunuk Wang,[a] Tae-Wook Kim[b] and Takhee Lee*[c]

Received 13th June 2011, Accepted 12th August 2011
DOI: 10.1039/c1jm12702k

In the past few decades, considerable progress has been made in the field of molecular electronics toward our understanding of charge transport processes and the development of experimental methods. This feature article presents a summary of various experimental characterisation platform testbeds for metal–molecule–metal junctions using self-assembled monolayer molecules. Important results from these techniques are highlighted here. A review of the mechanism of electronic transport through molecular layers is presented. Furthermore, the prospects and advanced architectures for the further development of molecular electronics are presented. These opportunities may contribute to the realisation of practical applications for molecular electronic devices.

1. Introduction

The interest in molecular electronics is grounded in the potential for individual or self-assembled monolayer (SAM) molecules to be used as functional electronic elements in different device applications.[1–23] One important application is the use of ultra-high-density electronic circuits as complements or alternatives to high-cost nanoscale Si-based integrated devices. In comparison to conventional Si-based technologies, molecular electronics could, in principle, offer numerous potential advantages. For example, a molecule in the size range of a nanoscale building-block could lead to a higher packing density for miniaturised electronic devices, enabling lower cost, higher efficiency, and fewer heat problems. Furthermore, with nanoscale self-assembly, it is possible to synthesise molecular structures with the desired functionality to form active structures. These advantages are expected to provide molecular electronics with the means to extend Moore's Law beyond the foreseen limits of miniaturising silicon integrated circuits.

Since Aviram and Ratner initially proposed the conceptual model of a unimolecular rectifier in 1974,[3] the field of molecular electronics has made tremendous progress in both experimental[24–44] and theoretical developments.[45–62] A wide range of electrical behaviour types for molecular junctions functionalised by individual or SAM molecules has been extensively investigated and reported, including diodes,[43,63–65] switches,[25,26,66–68] memory,[33,39,69–71] and transistors.[30,72,73] Furthermore, a variety of

[a]*School of Materials Science and Engineering, Gwangju Institute of Science and Technology, Oryong-Dong, Buk-Gu, Gwangju, 500-712, Korea*
[b]*Korea Institute of Science and Technology, Institute of Advanced Composite Materials, Jeollabuk-do, 565-902, Korea*
[c]*Department of Physics and Astronomy, Seoul National University, Seoul, 151-747, Korea. E-mail: takheelee@gmail.com; Fax: +82-2-884-3002; Tel: +82-2-880-8516*

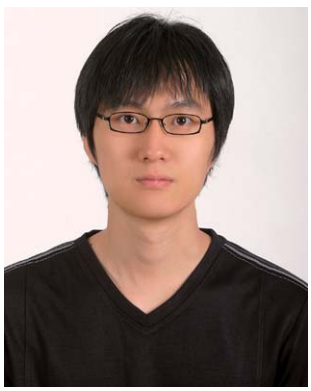

Gunuk Wang

Gunuk Wang is a PhD candidate in the School of Materials Science and Engineering, Gwangju Institute of Science and Technology (GIST), Korea. He graduated from Sungkyunkwan University, Korea and received an MS degree from GIST in 2007. Since then, he has investigated molecular electronic devices. Currently, his research interests focus on the charge transport mechanism and fabrication method for molecular electronic devices and on advanced architectures for practical device applications.

Tae-Wook Kim

Tae-Wook Kim is a senior research scientist at the Korea Institute of Science and Technology, Korea. He graduated from Pusan National University, Korea, and received his PhD degree from the Gwangju Institute of Science and Technology, Korea, in 2009. He was a postdoctoral researcher at the University of Washington, Seattle, USA, until 2010. His current research interests are organic memory devices, organic thin-film transistors, organic logic circuits, and carbon nanomaterials for organic electronics.

This journal is © The Royal Society of Chemistry 2011

platform and junction techniques, such as scanning probe microscope-based techniques,[34,36,38,40,56,74–77] break junctions,[24,30,72,73,78–80] crossed-wire tunnel junctions,[56,63,81–83] Hg drop junctions,[27,84–90] and various solid-state device-based methods,[25,26,32,33,37,39,43,44,55] have been developed to gain an understanding of molecular charge transport mechanisms. Nevertheless, there are still many issues and long-standing challenges that must be overcome before these molecules can be applied as actual electronic components in device circuits. For example, the creation of reliable molecular junctions continues to be challenging, and this will likely be the first milestone toward the practical development of molecular electronics. At the present time, inevitable limitations in available fabrication techniques, such as unstable junctions, low-yield device fabrication methods, ill-defined junction areas, and laboratory-dependent measurement data, lead to large variations in the intrinsic electrical properties of the materials produced, as we discuss in Section 2 of this article. These fabrication uncertainties have been major obstacles impeding our complete understanding of charge transport mechanisms in molecular devices and their application as electrical components in devices. Furthermore, it is necessary to synthesise or identify specific and robust molecular species that have prescribed electronic functionalities for the intended device components. To resolve these scientific and technical issues, the field of molecular electronics has rapidly developed in several areas. For example, better experimental testbeds have been developed, functional molecular species can now be synthesised, and the charge transport mechanism of molecular junctions is becoming better understood.

In this article, we present a review of the different experimental and theoretical aspects of molecular junctions, in which a few molecules (~100 molecules) or a bundle of molecules (up to $\sim 10^{12}$ molecules) are contained in a junction area ranging from 100 nm^2 to 500 μm^2. Several excellent reviews of single molecular electronic devices are available in the literature concerning the issues related to single-molecule devices, whereby one or very few molecules are contained in each junction.[16,22,91] In contrast, in this review article, we will focus on molecular junctions that use a bundle of molecules.

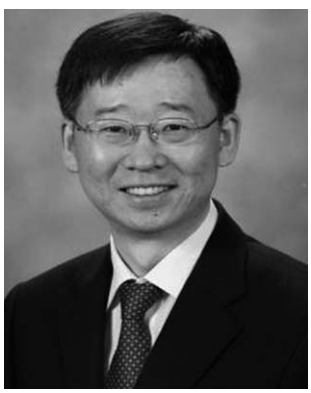

Takhee Lee

Takhee Lee is a faculty in the Department of Physics and Astronomy, Seoul National University, Korea. He graduated from Seoul National University, Korea, and received his PhD degree from Purdue University, USA in 2000. He was a postdoctoral researcher at Yale University, USA until 2004. His current research interests are molecular electronics, polymer memory devices, nanowire electronics, and graphene-electrode optoelectronic devices. He has written 9 book chapters, 8 review articles, and about 140 journal articles.

This article comprises four sections. Following a brief introduction of molecular electronics (Section 1), Section 2 describes various experimental testbeds that can be adopted to analyse the transport characteristics of molecular junctions, such as conducting probe atomic force microscopy (Section 2.1), crossed-wire junctions (Section 2.2), liquid metal junctions (Section 2.3), metal evaporated molecular junctions (Section 2.4), and conducting interlayer-based junctions (Section 2.5). In Section 3, several defects in molecular junctions are presented (Section 3.1), the specific charge transport characteristics of molecular junctions are presented in terms of molecular length-, structure-, and contact-dependent transport (Section 3.2); molecular conformation effects (Section 3.3); and transition voltage spectroscopic characteristics (Section 3.4). Section 4 provides a summary and some desired prospects for the further development of molecular electronics. Thus, this review article provides an overview of current issues in molecular electronics as well as the recent progress and important challenges related to this field.

2. Experimental testbeds for molecular junctions

2.1 Conducting probe atomic force microscopy

The conducting probe atomic force microscopy (CP-AFM) technique has been used by many research groups to characterise SAM molecules and to investigate their electrical properties.[40,56,92–97] In this testbed, a conducting AFM tip is directly applied to make top contact with the SAM molecules on bottom electrode substrates under a controlled loading force (Fig. 1(a)). A sweeping voltage is applied between the tip and the substrate in stationary mode to carry out electrical current–voltage (I–V) measurements. The CP-AFM technique has several merits. For example, direct contact on the SAM by an AFM tip can prevent the current reduction caused by the additional tunnelling gap that exists in scanning tunnelling microscopy (STM).[74–76,98] Additionally, this technique does not require the use of a device patterning process. However, variations in the AFM tip radius and bottom electrode roughness induce some uncertainty in the number of molecules in the junction, resulting in a large variation in the measured I–V characteristics.[99,100] Note that with an Au nanoparticle on the mixed SAM (*e.g.*, alkanethiol and alkanedithiol molecules), it is possible to reproducibly measure the single alkanedithiol molecular conductance without the effect of variations in the junctions because the Au particles are only attached to the inserted alkanedithiol molecules in the mixed monolayer.[96,101,102]

2.2 Crossed-wire junction

A schematic of a crossed-wire junction is shown in Fig. 1(b). This junction technique consists of two Au wires that are approximately 10 μm in diameter.[56,63,81–83] The molecular species of interest are self-assembled on one of the Au wires, which is placed orthogonal to an applied magnetic field. The contact in this junction structure is completed by deflecting the Au wires with a Lorentz force generated from a small DC current (under a few mA). The electrical I–V characteristic is measured by applying a sweeping voltage between both wires. In this technique, it is possible to use different wire compositions to study asymmetric junctions.[103] Furthermore, this technique enables the

 This journal is © The Royal Society of Chemistry 2011

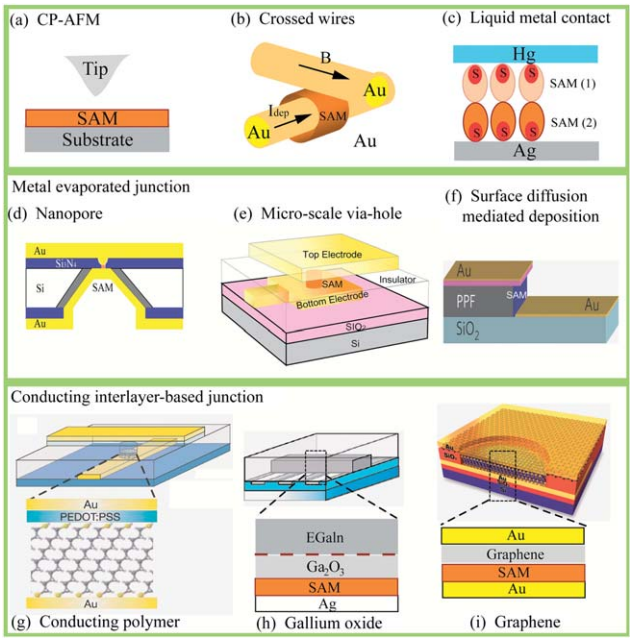

Fig. 1 Examples of molecular junction platforms. (a) CP-AFM, (b) crossed-wires, (c) liquid metal contact junction, metal evaporated junction ((d) nanopore, (e) microscale *via* hole junction, and (f) surface diffusion mediated deposition). Conducting interlayer-based junctions ((g) conducting polymer-based, (h) gallium oxide-based, and (i) graphene-based junctions). Reprinted with permission: (d) from ref. 109, © 2003, The American Physical Society; (e) from ref. 119, © 2008, American Chemical Society; (f) from ref. 123, © 2010, Nature Publishing Group; (g) from ref. 37, © 2006, Nature Publishing Group; (h) from ref. 129, © 2010, American Chemical Society; (h) from ref. 44, © 2011, Wiley-VCH Verlag GmbH & Co. KGaA, Weinheim.

investigation of a scaling effect on electronic charge transport *via* the sensitive modulation of the deflection current.[82,104] More molecules are contacted by both metallic wires when the deflection current is increased. However, the number of contacted molecules and their orientation on the wire are not well defined because of the surface curvature of the wire.

2.3 Liquid metal contact

Hg–SAM–SAM–metal junctions are fabricated by controlling a drop of SAM-coated Hg with a second metal surface (Ag, Au, Cu, or Hg) that contains another SAM (Fig. 1(c)).[27,84–90] This molecular junction technique has several merits due to the defect-free surface of liquid metal Hg and the bi-layer SAMs.[27,84–86] For example, the Hg contact in the junction prevents problems encountered with evaporating metal top-contacts, such as the issue of the upper metal penetrating into the junction. Therefore, it is convenient to measure numerous electrical datasets at different contact sites. In fact, the simplicity of this technique will ensure the validity of statistical analysis of the data and enable the understanding of charge transport mechanisms. However, the roughness of the second (bottom) metal surface leads to abrupt changes in the distance between the two electrodes, generating uncertainty in the contact area.[99] Furthermore, the junction yields are low (under 25%) and the junctions may be unstable[43] because Hg is easily amalgamated with the bottom electrodes (*e.g.*, Ag and Au) during repeated *I–V* measurements and subsequent aging, which may lead to a short circuit.[105–108]

2.4 Metal evaporated molecular junction

2.4.1 Nanopore. The SAM in a nanopore junction is sandwiched between two metallic contacts, as illustrated in Fig. 1 (d).[25,35,69,109–112] This junction technique is a solid-state device platform that contains a number of molecules (several thousand) in a nanoscale hole (typically 40–50 nm in radius). Subsequently, electron beam lithography and reactive ion etching create a single pore with a diameter in the tens of nanometres through the suspended isolating layers, such as Si_3N_4 and SiO_2. After the formation of a SAM on the evaporation side (top) electrode, the second metallisation on the other side (bottom) is performed to complete the molecular junction. To avoid thermal damage to the SAM layer, liquid nitrogen is kept flowing throughout the cooling stage, and the evaporation rate is kept very low. Although this technique reduces the kinetic energy of the evaporated metal atoms on the SAM layer, the yield of nanopore devices is still low due to the high possibility of short circuit formation *via* the punching of metal atoms through the SAM layer.[18,113–115] However, this junction technique allows temperature variable measurements, which is very useful for identification of the main charge transport mechanism.[109] The number of molecules in the junction is well known because the contact area can be measured accurately by scanning electron microscopy (SEM), permitting the current (or resistance) per molecule to be measured with a high degree of accuracy. This technique is a useful platform for the demonstration of functional device applications, such as molecular memory and diodes.[69,116]

2.4.2 Microscale *via*-hole junction. The microscale junction is fabricated on a p-type (100) Si substrate covered with a thermally grown >100 nm-thick layer of SiO_2 (Fig. 1(e)).[55,117–119] This junction technique has a fabrication process that is quite similar to the nanopore junction technique, except that lithography is used for hole formation at the junction. Therefore, the merits and demerits of microscale junctions are similar to those of nanopore junctions. Due to the microscale hole (2 to 4 μm diameter) in the junction, it is possible to easily and quickly fabricate a large number of molecular devices using conventional optical lithography. This junction technique also involves the evaporation of metal onto the molecules at the top electrode. Evaporation may cause electrical short-circuit problems as well as unstable and unexpected *I–V* characteristics due to the creation of filamentary paths and molecular damage.[18,113–115,117,120–122] This inevitable uncertainty in the fabrication technique leads to relatively large variations in the junction conductance, despite the use of identical molecular components. This uncertainty is an obstacle for the understanding of molecular charge transport mechanisms and has potential implications for future device applications. Therefore, new techniques and ideas have been developed to resolve this issue (Fig. 1(f)–(i)). In the following section, we present a review of these new device techniques, which have a more stable and higher junction yield.

2.4.3 Surface diffusion mediated deposition. A schematic of a molecular junction technique using surface diffusion-mediated

deposition (SDMD) is shown in Fig. 1(f).[123] This junction technique has been completed through four fabrication processes: PPF (pyrolyzed photoresist film) fabrication, PPF-side wall fabrication, molecular layer deposition, and metal contact deposition.[123] To form PPF, a 300 nm SiO_2/p-Si substrate was spin coated with photoresist (AZ P4330–RS) and decomposed (pyrolyzed) by heating in a tube furnace. Optical lithography and lift-off technique were used to pattern etch mask (SiO_2/Cr) on the PPF layer. Then, an O_2 reactive ion etch (RIE) process was used to remove the PPF layer that was not protected by the patterned etch masks, and an anisotropic etching condition was selected to create the formation of a near vertical sidewall. Then, a molecular monolayer was attached to the PPF sidewall by means of electrochemical reduction or oxidation in solution. For SDMD, metal contacts were deposited by electron beam evaporation through a shadow mask aligned perpendicular to the patterned SiO_2/Cr mask. Electrical connection between the metal and the molecules is completed by surface diffusion of the deposited metal atom toward the molecular layer. This junction technique has several merits. For example, the SDMD technique prevents the problem of penetration and damage by evaporated metal atoms, which leads to the excellent yield (>90%) and reproducibility of molecular junctions. In addition, the contact region of the molecule/metal is controlled though surface diffusion of the deposited metal atom that depends on the thickness of the metal, which can allow characterization of a wide range of molecular junctions from single/several molecules to many molecules. However, it may be difficult to know the accurate junction area and the exact number of molecules in the junction. And, the charge transport study through molecular layers with various contact groups may have some limitation because of the PPF bottom electrode's surface.

2.5 Conducting interlayer-based molecular junction

2.5.1 Conducting polymer interlayer-based junction. A schematic of the conducting polymer-based junction structure is shown in Fig. 1(g).[37] This junction technique involves an insulating photoresist layer on top of the patterned bottom electrodes to electrically isolate the molecular junction, which allows good contact with the conducting polymer and prevents degradation of the device in ambient conditions.[37,68,124,125] Holes in the photoresist layer have diameters in the several tens of micrometres for conventional optical lithography (up to ~100 μm diameter). After SAM formation on the bottom electrode, a water-based suspension of conducting polymer PEDOT:PSS (poly-(3,4-ethylenedioxythiophene) stabilised with poly-(4-styrenesulfonic acid)) is spin-coated on top of the SAMs, covering the complete device. The thickness of the PEDOT:PSS layer is typically 200 to 300 nm, preventing the formation of electrical shorts upon subsequent deposition of the Au top electrode. Furthermore, it is possible to adjust the conductivity of PEDOT:PSS (20–300 S cm^{-1}) *via* the addition of a polar solvent, such as dimethylsulfoxide (DMSO).[126] Subsequently, the Au top electrode (thickness: 50–100 nm) is deposited on top of the PEDOT:PSS layer through a shadow mask. RIE with O_2 is used to remove the redundant PEDOT:PSS. The Au top electrode is used as a contact with the probes and as a shadow mask, whereas PEDOT:PSS is etched away using RIE to prevent a direct current path through PEDOT:PSS from the Au top electrodes to the Au bottom electrodes. The fabrication of large-area molecular devices using PEDOT:PSS as an interlayer between the top electrode and these molecules has been one of the most successful techniques in terms of high device yields and stable junctions.[37] Nevertheless, the use of a conductive polymer has some limitations and presents some uncertainties as a universal platform for physical–organic studies because the properties of the interface between the polymer layer and the molecules are still not well understood.[37,43,124,127,128] For example, the resistance of materials fabricated using this technique has been reported to differ significantly from that of molecular junctions that do not have the conducting polymer interlayer due to relatively poor contact between PEDOT:PSS and the molecules.[127,128] Additionally, the yield of the polymer interlayer-based junction system seems to depend on the type of isolating layer (photoresist or SiO_2) and on the molecular contact groups (hydrophilic or hydrophobic) due to differences in surface tension.[37,124,127]

2.5.2 Gallium oxide interlayer-based junction. A schematic of the Ga_2O_3-based junction structure is shown in Fig. 1(h).[43,129] This junction technique incorporates a template-striped Ag (Ag^{TS}) bottom electrode to reduce the density of defects in the SAM by utilising the low surface roughness and large grain size of an Ag^{TS} electrode.[99] After the SAM forms on the Ag^{TS} electrode, a layer of Ga_2O_3/EGaIn suspended from a syringe contacting the SAM is deposited as the top electrode. The junction area ranges in area from 100 to 500 μm^2. The Ga_2O_3 interlayer, which is formed by oxidation of EGaIn, is only a few atomic layers thick (1 to 2 nm) and is stable. The Ga_2O_3 layer is expected to form a van der Waals interaction with the terminated group of the SAM. Furthermore, the resistance of the Ga_2O_3 layer is estimated to be several orders of magnitude less than the total resistance of the molecular junction. Thus, the Ga_2O_3 layer can be regarded as a conducting interlayer.[129] This molecular junction technique has several advantages.[129] For example, it does not require metal deposition directly on the SAMs. Furthermore, the junction is quite stable and easy to fabricate. However, there are some uncertainties due to the Ga_2O_3 protective layer in the molecular junction.[43,129] For example, the physical and chemical properties of the Ga_2O_3 layer are ill-defined with respect to the morphology and resistivity of the Ga_2O_3 layer, as well as the interface properties between the Ga_2O_3 layer and the SAM. These uncertainties may introduce difficulties in the interpretation of electrical data for the molecular junctions.

2.5.3 Graphene interlayer-based junction. A schematic of a graphene-based junction structure is shown in Fig. 1(i).[44] Graphene is an ultra-thin, two-dimensional sheet of covalently bonded carbon atoms. This material has outstanding electronic properties, chemical stability, and mechanical properties.[130,131] It is considered a good electrode candidate for molecular junctions. Large-area, conductive, and flexible graphene films have been successfully synthesised and patterned to desired sizes and shapes.[131] After the molecules are self-assembled on an exposed few micrometre-diameter Au bottom electrode, a multi-layer graphene (MLG) film (average thickness <~10 nm) is transferred to the substrate as the top electrode. The MLG film can be prepared by chemical vapour deposition (CVD), which produces

 This journal is © The Royal Society of Chemistry 2011

a typical sheet resistance of ~600 Ω □$^{-1}$ and a transmittance of ~87% in the visible wavelength range.[132–134] Next, an Au layer is vapour-deposited on top of the graphene films using a shadow mask at a low deposition rate. This layer reduces the sheet resistance of the graphene films during electrical probing. The graphene interlayer electrode prevents the formation of electrical shorts and filamentary paths that would result from penetration of the Au top metal. Fabrication of the molecular devices is completed by RIE to remove the redundant graphene films on the devices. This junction technique produces excellent durability, thermal and operational stabilities, and device lifetimes.[44] Furthermore, the yield of this junction technique has been found to be >~90%, regardless of the properties of the isolating layer and contact groups (hydrophobic *vs.* hydrophilic). In addition, the electronic coupling of graphene to the molecules seems to be better than that of PEDOT:PSS, resulting in a better contact conductance. However, the use of a graphene interlayer in this system has some limitations at the nanoscale *via* hole junction due to the limited flexibility of the MLG film. The structure of our MLG-interlayer based molecular junction includes an insulating layer (SiO_2, ~100 nm) for isolation of the SAM layer which is deposited on top of the bottom Au electrode (red layer in Fig. 1(i)). In the nanoscale *via* hole junction, it may be difficult for the MLG film to contact the SAM layer at the edge of the nanohole (or at the entire area of the nanohole) when the thickness of SiO_2 layer is comparable to (or larger than) the diameter of the nanohole. In other words, the transferred MLG film on substrate may be suspended across the SiO_2 layer around the nanohole due to the limited flexibility of the MLG film, which may lead to a low yield of molecular junctions. Therefore, in order to fabricate the nanoscale junction with graphene interlayer, it is necessary to reduce the thickness of the insulating layer or to use a single graphene layer that has more flexibility than the MLG film for completed contact between the graphene film and the SAM layer.

3. Electronic transport of molecular junctions

3.1 Defects in molecular junctions

Generally, the structure of SAM in the junction contains several types of defects.[12,99,135] The cause of defects can be an intrinsic or extrinsic factor: cleanliness, roughness, and type of bottom substrate (metal and semiconductor), type of top electrode, method for deposition of the top electrode, methods for SAM formation on substrate, and purity of SAM. These result in a complex phase than defect-free highly ordered SAM arrangement in the junction.[12] Recently, Nijhuis *et al.* summarized several possible defects in the Ga_2O_3 interlayer-based molecular junction in terms of local defects of "thin-area" or "thick-area," according to the local distance between the top and bottom electrodes that determines the junction conductance (Fig. 2).[135] Thin-area defects occur when the contact between the top electrode and the SAM on bottom electrode is disordered, and the distance between the electrodes is less than the length of molecules. For example, step edges, vacancy islands, and grain boundaries on the bottom electrode surface result in thin-area of SAM (Fig. 2(a) and (b)). Furthermore, different orientation of SAM and impurities within the electrode film will cause disorder

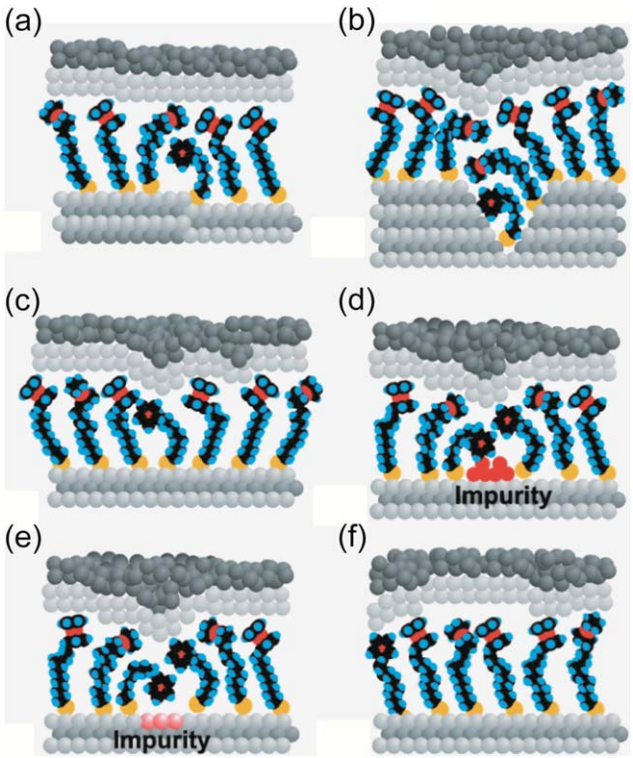

Fig. 2 Schematic of several possible defects in Ga_2O_3 interlayer-based molecular junction: (a) step edges and vacancy island on bottom electrode surface, (b) grain boundaries on bottom electrode surface, (c) different orientation of the molecular chains, (d) and (e) impurities in bottom electrode surface, and (f) non-conformal contact of the top electrode with the SAM. Reprinted with permission from ref. 135, © 2010 American Chemical Society.

in the SAM (Fig. 2(c)–(e)), which also leads to thin-area of SAM. This type of defect results in a high value of tunneling conductance due to the reduction of distance between the electrodes. However, thick-area defects occur when the top electrode of Ga_2O_3 does not make conformal contact with the SAM and the solute molecule or dust separates the top electrode and the SAM (Fig. 2(f)), which leads to low value of tunneling conductance because of the increase in distance between the electrodes. Consequently, these defects in the molecular junctions become the immediate cause of ill-defined *I–V* characteristics, large variation in the junction conductance, and the electrical short circuit formation with evaporated top metal atoms.

3.2 Molecular length-, structure-, and contact-dependent transport characteristics

In molecular electronics, the most studied issues are the influence of molecular length, structure, and contact dependence on the current–voltage (*I–V*) characteristics of molecular junctions. The non-linear *I–V* characteristics of molecular junctions containing various types of molecular components have been extensively investigated with a variety of platforms and techniques.[24–44,63–90] In this section, we present a review of electronic transport properties through different types of SAM molecules in various

molecular junction structures in terms of molecular length, structure, and contact groups.

A large number of microscale molecular devices (27 840 devices in total) were fabricated and characterised to statistically analyse the molecular electronic properties of a sufficient number of "working" molecular electronic devices (427 devices) (Fig. 3).[55] The molecular system in this study is the extensively studied alkanethiol, whose structure and configuration are sufficiently well characterised such that the system can serve as a standard.[6,12,136,137] There are two kinds of alkanethiols, alkanemonothiols ($CH_3(CH_2)_{n-1}SH$) where one thiol is located at the end of the molecule, and alkanedithiols ($HS(CH_2)_nSH$) where thiols are located at both ends of the molecule. This molecular system presents a simple classical molecular tunnel junction when fabricated between metallic contacts, due to the large highest occupied molecular orbital (HOMO)–lowest unoccupied molecular orbital (LUMO) gap of approximately 8 eV.[9,109,138] The "working" molecular electronic devices were extracted from devices showing a majority of the current densities in the statistical distribution, by using a Gaussian function (Fig. 3(a)–(f)). In fact, determination of the average transport parameters from a statistically meaningful number of working molecular junctions is a prerequisite because statistically averaged transport parameters can provide more accurate and meaningful characteristics of molecular systems. The importance of statistical analysis that is based on a large amount of electrical data has grown in recent years due to reliability issues with molecular junctions.[21,37,39,43,44] The detailed criteria used for determining working devices have been reported in the literature.[117] The device yields were found to be ~1.2% (156/13 440 devices) for alkanemonothiol devices and ~1.9% (271/14 440 devices) for alkanedithiol devices. Because the device yield (~1.75%) of DC8 ($HS(CH_2)_8SH$) devices did not differ much from that of C8 ($CH_3(CH_2)_7SH$) devices (~1.41%), it is not likely to be greatly affected by metal–molecule contact but, rather, is affected more by the device structure, fabrication condition, and quality of the SAM molecules (the packing density and defect sites in SAM layer on bottom electrode).[12] Fig. 3(a)–(f) present histograms of the current densities for different lengths of alkanemonothiols (C8, C12, and C16) and alkanedithiols (DC8, DC9, and DC10) at 1.0 V with the mean positions of representative devices indicated with arrows. The current density–voltage (*J–V*) characteristics for these six representative devices are plotted in Fig. 3(g). The main conduction mechanism through the alkanethiol molecular devices is the non-resonant tunnelling mechanism, which was demonstrated by its temperature-independent *I–V* characteristics and the exponential dependence of its transport characteristics on molecular length.[117] The histograms in Fig. 3(a)–(f) show the distribution of the logarithmic current densities, indicating the existence of fluctuation factors causing the exponential distribution in J, such as fluctuations in the molecular configuration or microstructures in the metal–molecule contacts.[139,140] The *J–V* characteristics in Fig. 3(g) were clearly dependent on the exponential molecular length and metal–molecular contacts (*i.e.*, monothiol *vs.* dithiol). This observation was supported by previous reports of molecular junctions that have shown that the *J* for alkanedithiols is higher than that for alkanemonothiols due to the different natures of their metal–molecule contact properties (chemisorbed *vs.* physisorbed contact) at Au-molecule contacts.[94,96]

Similar exponential length-dependent and temperature-independent *I–V* characteristics of alkanethiol SAM molecules were also observed from other molecular junction structures using an interlayer of high-conducting materials, such as PEDOT:PSS[37,124] or graphene layers,[44] between the top metal and the SAM molecules (Fig. 4). These results demonstrate that PEDOT:PSS and graphene can be regarded as non-interacting conductive electrodes. As mentioned above, the yield of molecular junction structures without an interlayer is very low (Fig. 1(d) and (e)), mainly because of electrical shorts caused by the top electrode penetrating through the molecular layer and making contact with the bottom electrode. However, an interlayer of PEDOT:

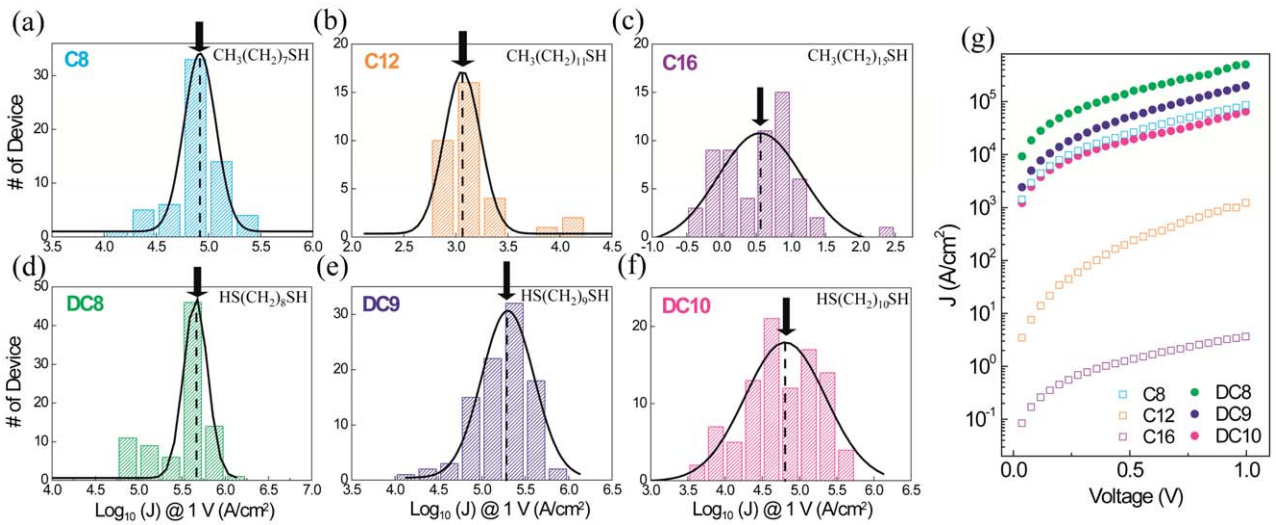

Fig. 3 Statistical histograms of log *J* measured at 1.0 V for (a) C8, (b) C12, (c) C16, (d) DC8, (e) DC9, and (f) DC10. The line curves are fitted results obtained from the histograms with Gaussian functions and the mean positions are indicated with arrows. (g) *J–V* characteristics of representative devices chosen from the mean positions of the fitted Gaussian function. Reprinted with permission from ref. 55, © 2007, The American Physical Society.

 This journal is © The Royal Society of Chemistry 2011

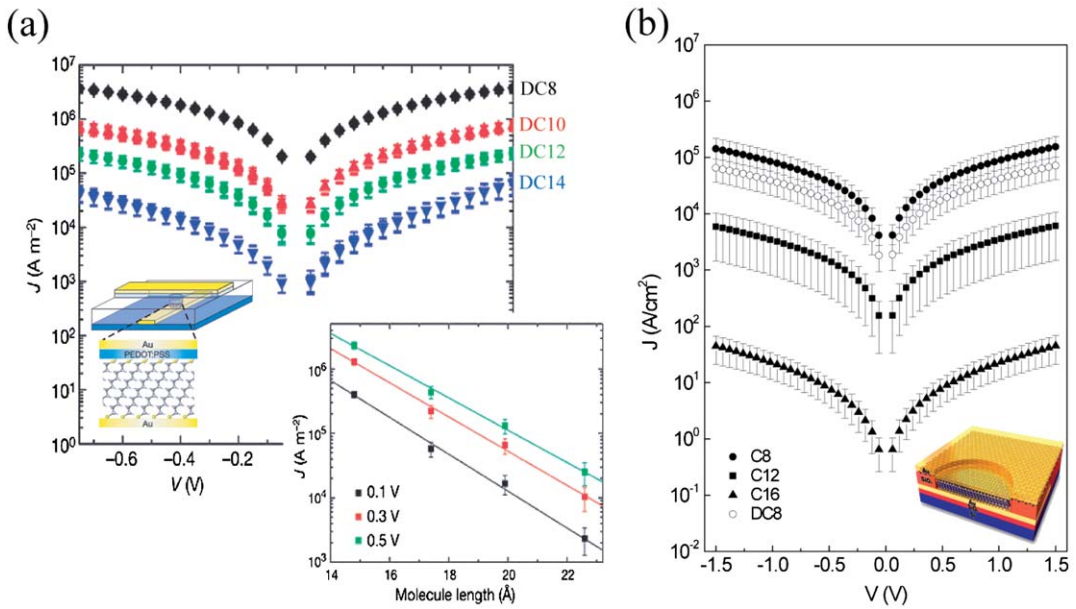

Fig. 4 (a) The *J–V* characteristics for the PEDOT:PSS-based alkanedithiol (DC8, DC10, DC12, and DC14) junction. The inset shows the *J–d* (molecular length) plot in the low bias region. Reprinted with permission from ref. 37, © 2006, Nature Publishing Group. (b) The *J–V* characteristics for graphene-based alkanedithiol (DC8, DC12, and DC16) and alkanemonothiol (C8) junctions. Reprinted with permission from ref. 44, © 2011, Wiley-VCH Verlag GmbH & Co. KGaA, Weinheim.

PSS or graphene film can effectively prevent the formation of electrical shorts and filamentary paths that result from penetration of the Au top metal, producing an excellent device yield (>90%) and high reproducibility. In addition, the current level in these interlayer molecular devices has been found to be stable for at least 40 days in air.[37,44,125]

Let us examine the electrical characteristics of graphene-based molecular junctions in more detail. As shown in Fig. 4(b), the difference in the conductance of C8 and DC8 in graphene-based molecular junctions (Fig. 4(b)) can be explained by a difference in the properties of the physisorbed contacts, corresponding to different contact lengths. This difference occurs because the graphene electrode does not form a chemisorbed contact with thiol (–S). Therefore, the conductance of the C8 junction is higher than that of the DC8 junction due to the shorter contact length of the C8 junction (contact length $d_{[CH3/graphene]}$ for C8 < $d_{[C–S/graphene]}$ for DC8).[44,55,141]

To demonstrate the quality of the contact transport property, the charge transport parameters for DC8 molecular junctions were compared according to the type of top electrode (PEDOT:PSS, graphene, and Au) (Fig. 5).[44] Fig. 5(a) shows a histogram of the current densities at 1.0 V on a logarithmic scale, and Fig. 5(b) shows R_{mol} (resistance per molecule) for different types of top electrodes. The resistance for Au/DC8/graphene was slightly higher than that for Au/DC8/Au devices by less than one order of magnitude (Fig. 5(b)). Unlike the relatively poor contact between DC8 and PEDOT:PSS (with much more resistance in the Au/DC8/PEDOT:PSS case), the contact between graphene and DC8 was comparable to that between Au and DC8 (Fig. 5(a) and (b)). This difference can also be observed in different types of junction systems. For further details regarding this issue, we recommend Akkerman's review paper,[128] which compares conductance results with several experimental techniques.

In molecular junctions, the most common finding is that resistance (R) increases exponentially with molecular length (d), according to eqn (1):[9,37,44,55,92–95]

$$R(d) = R_o \exp(\beta d) \quad (1)$$

where R_o is an effective contact resistance that depends on the anchoring group and contact electrodes and β is the decay factor that depends on the nature of the molecular structure and the bias voltage. Generally, β is determined by taking the linear fit of a logarithmic plot of the resistance *versus* different molecular lengths (Fig. 6). This physically reflects the extent of the decrease in wave function for the tunnelling charge through the molecular structure.[44] The small HOMO–LUMO gap for π-bonded molecules (3–5 eV),[9,56,95] compared with that of alkanethiol molecules (~8 eV),[9,109,138] explains the noticeable difference in β values between the two molecules and the greater conductance through molecules of the former. For example, the β values were found to be ~0.92 Å^{-1} for alkanethiol molecules (Fig. 6(a)),[55] which is higher than that for π-bonded ones (such as oligoacene and oligophenylene derivatives) (Fig. 6(b)–(d)).[92,95,142] Typical β values range from 0.2–0.6 Å^{-1} for π-bonded molecules and 0.6–1.2 Å^{-1} for alkanethiol molecules.[9,87,92,95,143] As mentioned above, the β value is dependent on the molecular structure (~0.92 Å^{-1} for alkanethiol molecules, Fig. 6(a); ~0.2 Å^{-1} for *para*-phenylene molecules, Fig. 6(b); and ~0.5 Å^{-1} for oligoacene-based molecules, Fig. 6(c)), but it is not quite as dependent on metal–molecule contacts (*i.e.*, monothiol *vs.* dithiol and –S *vs.* –NC) (Fig. 6(a)–(c)). Noticeably, the β values for the phenylenes in PEDOT:PSS-based junctions were found to be lower than the reported values in the literature (*i.e.*, β = 0.35–0.61 Å^{-1}).[36,87,92,144,145] One reason for this finding may be the influence of the monolayer on the molecular geometry. The β values have

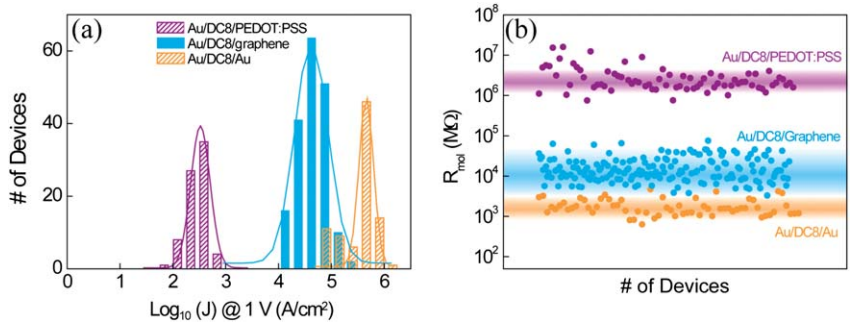

Fig. 5 (a) Histogram of logarithmic J at 1 V for molecular devices with different types of top electrodes (PEDOT:PSS, graphene, or Au). (b) The resistance per molecule R_{mol} values for these molecular junctions. Reprinted with permission from ref. 44, © 2011, Wiley-VCH Verlag GmbH & Co. KGaA, Weinheim.

been found to be as low as 0.17 and 0.24 $Å^{-1}$ for planar *para*-phenylene systems (molecular systems with no torsion angle between adjacent phenyl rings).[146,147] Furthermore, higher per-molecule resistances R_{mol} were observed experimentally and calculated theoretically for alkanethiol molecules than for π-bonded molecules of comparable lengths or slightly

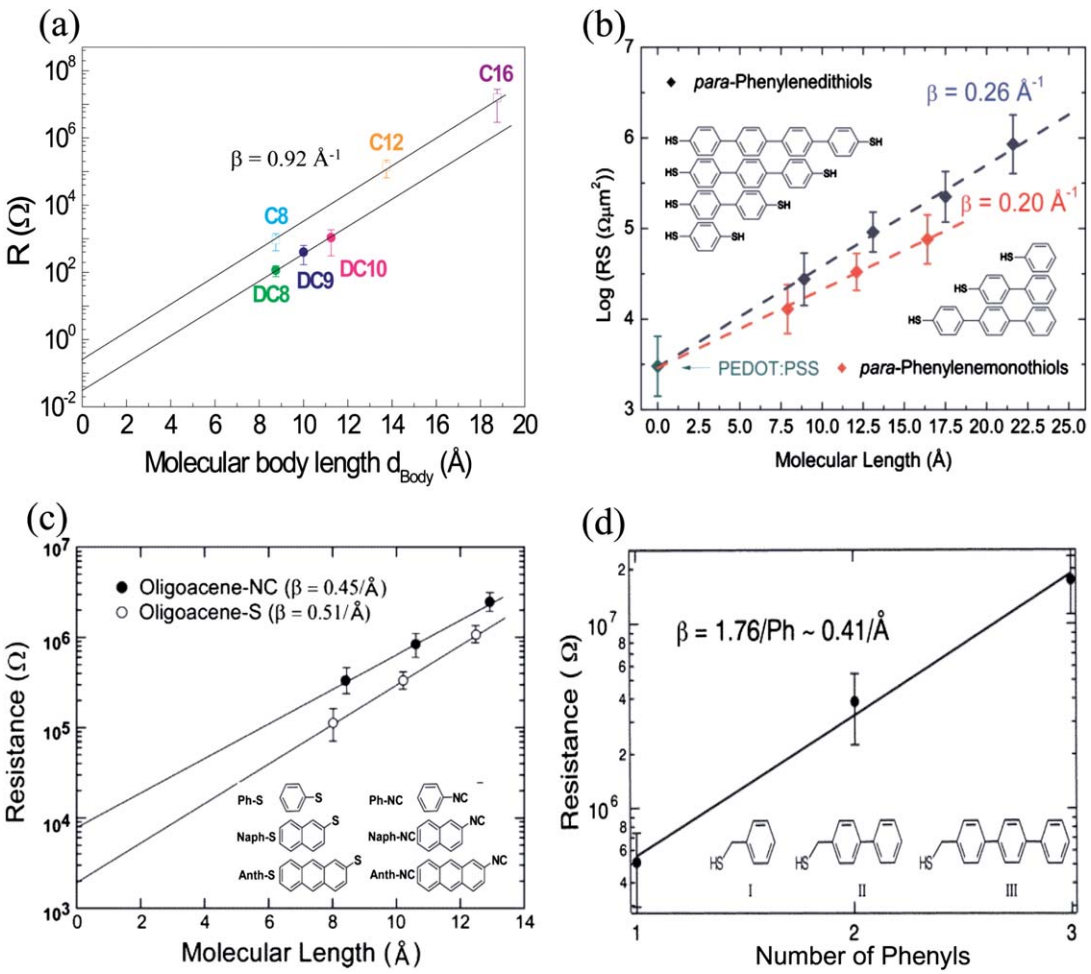

Fig. 6 (a) Semilog plot of R *versus* d_{body} for alkanemonothiol and alkanedithiol junctions on the microscale *via* a hole junction platform. Reprinted with permission from ref. 55, © 2007, The American Physical Society. (b) Normalised resistance log (R_S) *versus* d plot for P1DT–P4DT and P1MT–P3MT in PEDOT:PSS-based molecular junctions. Reprinted with permission from ref. 142, © 2010, American Institute of Physics. (c) Semilog plot of R *versus* d for oligoacene-S and oligoacene–NC in a CP-AFM junction platform. Reprinted with permission from ref. 95, © 2006, American Chemical Society. (d) Semilog plot of R *versus* N (number of phenyl groups in SAMs of I–III) for oligophenyl-based molecules in a CP-AFM junction platform. Reprinted with permission from ref. 92, © 2002, American Chemical Society. Straight lines show linear fits of the data, giving the β values.

 This journal is © The Royal Society of Chemistry 2011

longer.[9,55,92,95,119,142] These comparisons provide a clear indication that alkanethiol molecules in molecular junctions indeed have a significantly higher tunnelling barrier height than do π-bonded ones. In other words, these molecules have lower tunnelling charge efficiency for alkanethiol molecular junctions.

The contact resistance R_o can be utilised in investigating metal–molecule contacts, which can be defined in the limited condition (*y*-intercept in Fig. 6) when molecular length (*d*) approaches zero. The results in Fig. 6(a)–(c) indicate that (1) R_o for alkanedithiols is smaller than R_o for alkanemonothiols by roughly an order of magnitude due to the different properties of chemisorbed and physisorbed contacts;[55] (2) R_o for oligoacene-SH is smaller than R_o for oligoacene-NC due to the presence of a higher tunnelling barrier at the contact for isocyanide (CN)-linked molecules than for thiol (S)-linked ones;[95] (3) R_o for *para*-phenylenedithiols and R_o for *para*-phenylenemonothiols have similar values, coinciding with the junction resistance without a SAM (*i.e.*, PEDOT:PSS by itself; Fig. 6(b)).[142] This similarity indicates that R_o is dependent on the molecular anchoring groups (*i.e.*, monothiol *vs.* dithiol and –S *vs.* –NC) and on the molecular junction structures.

Next, we will provide more information concerning the decay factor β and the contact resistance R_o. As shown in Fig. 7(a), no trends were found in the measured β values with work function for contact electrodes for alkanemonothiol or alkanedithiol devices.[94] Furthermore, the β values, with standard deviations obtained from a variety of junction structures, were within a range of similar values (Fig. 7(b)).[37,43,44,55,86,87,93,94,109,148] Unlike the contact-independent β values for both alkanemonothiols and alkanedithiols, the R_o values for alkanemonothiol and alkanedithiol junctions were observed to decrease when the work function of the contact metal increased (Fig. 8).[94] The trend of decreasing R_o with increasing metal work function indicates a hole-type transport in alkanethiol molecular junctions, whereby the HOMO level more closely aligns with the Fermi level E_F of the metal than the LUMO level. In this case, the E_F approaches the HOMO level as the metal work function increases, thereby decreasing the contact barrier height to transport through the junction and reducing R_o. Moreover, the R_o values were found to be different for asymmetric metal contacts (*e.g.*, [Ag/Au] and [Au/Ag]) for alkanemonothiols because of the different natures of metal–molecule contacts (physisorbed *vs.* chemisorbed on the contact side). However, R_o values for alkanedithiols were found to be the same for asymmetric contacts due to the identical nature of the metal–molecule contact.[94,119]

As mentioned above, the fundamental properties of SAM molecules in molecular junctions are their resistance (or conductance) and decay factors, which allow for direct examination and understanding of the charge transport mechanism. Recently, the systematic length dependence of charge conduction on short (<4 nm) and long conjugated molecules (up to 7.3 nm in length) was studied using the CP-AFM technique.[40] Variable lengths of conjugated oligophenyleneimine (OPI) molecules bonded to Au electrodes through a thiol-linkage were synthesised by controlled aryl imine addition chemistry (Fig. 9(a)).[40] Based on various lengths of the conjugated OPI molecules (1.5 to 7.3 nm), a change in transport mechanism from tunnelling to hopping in molecular junctions was demonstrated. Fig. 9(b) shows a semilog plot of resistance *R versus* molecular length *d*, with decay factor β. Notably, transitions in the length dependence of resistance and the decay factor were observed near 4 nm (OPI 5). The β value for short OPI molecules (OPI 1 to 4) was found to be 0.3 $Å^{-1}$, which is within the range of β values (0.2–0.6 $Å^{-1}$) for typical conjugated molecules. For long OPI molecules, a much smaller β value of ~0.09 $Å^{-1}$ and a flatter semilog plot of *R versus d* were observed (Fig. 9(b)). These results indicate

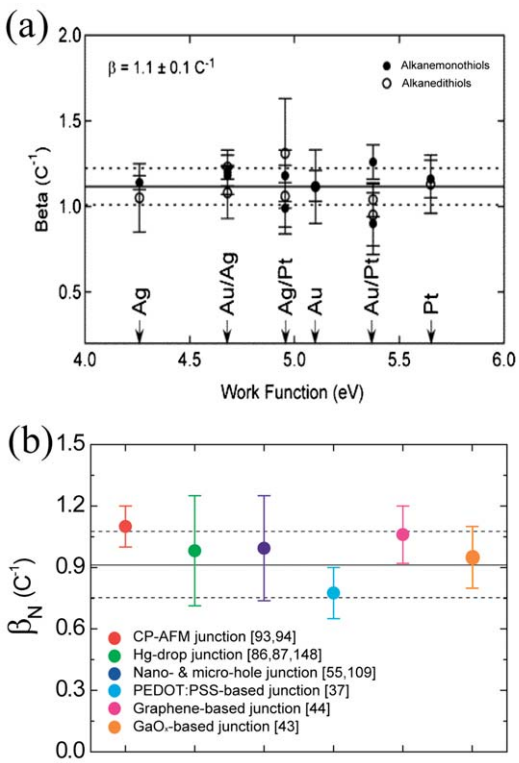

Fig. 7 (a) The β values as a function of electrode metal work functions for alkanemonothiols (●) and alkanedithiols (○) in a CP-AFM junction. Reprinted with permission from ref. 94, © 2004, American Chemical Society. (b) The β values of alkyl-based molecular junctions in different testbeds.[37,43,44,55,86,87,93,94,109,148]

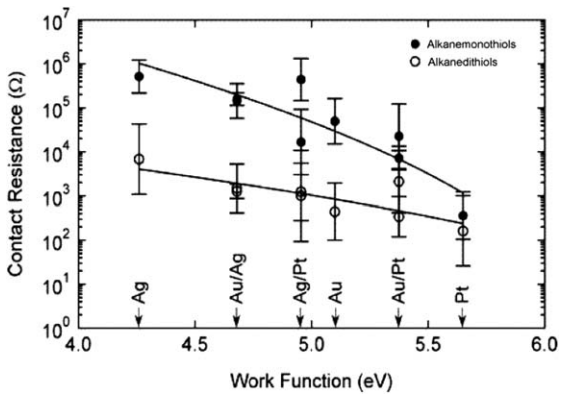

Fig. 8 Contact resistance R_o as a function of electrode metal work function for alkanemonothiols (●) and alkanedithiols (○) in CP-AFM junctions. Reprinted with permission from ref. 94, © 2004, American Chemical Society.

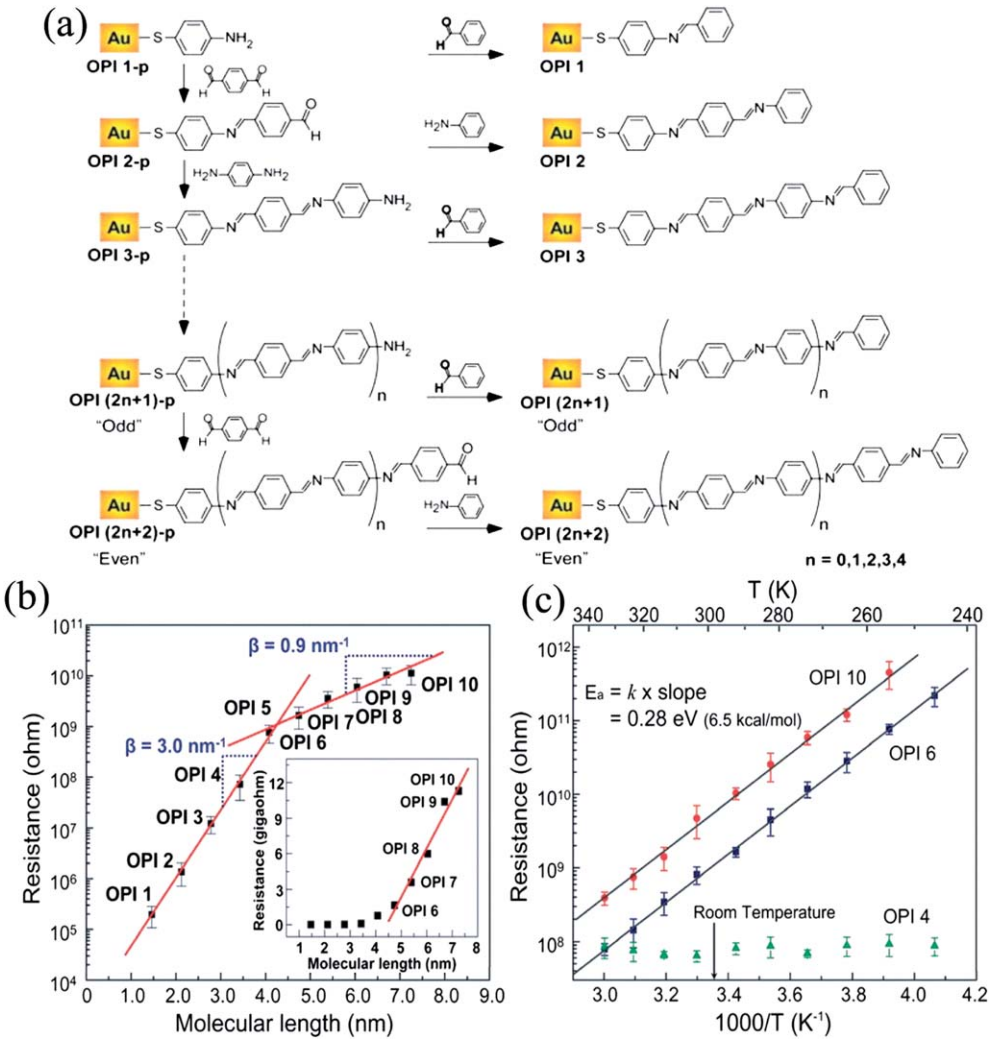

Fig. 9 (a) Molecular structure and synthetic route to OPI-p and OPI monolayers on Au substrates. Measurements of R in CP-AFM junctions. (b) Semilog plot of R *versus* d for these molecular junctions. The two straight lines are linear fits to the data, giving two regimes of β values. The inset shows a linear plot of R *versus* d, demonstrating linear scaling of R with d for the long OPI wires. (c) Arrhenius plot for OPI 4, OPI 6, and OPI 10. Straight lines are linear fits to the data, giving the activation thermal energy. Reprinted with permission from ref. 40, © 2008, American Association for the Advancement of Science (AAAS).

that the conduction mechanism is different in short (OPI 1 to 4) and long (OPI 6 to 10) OPI molecules. The change in the conduction mechanism was directly verified by the measurement of temperature-dependent resistances for short and long OPI molecules. Fig. 9(c) shows a plot of resistances for short (OPI 4) and long OPI molecules (OPI 6 and 10) as a function of temperature. The short OPI 4 molecule exhibited tunnelling transport that was independent of temperature, while the long OPI 6 and 10 molecules exhibited strongly thermally activated (hopping) transport. The activation energy E_a for the long molecules OPI 6 and OPI 10 was obtained by the slopes shown in Fig. 9(c) and found to be identical (both ~0.28 eV). These experimental results enable investigation into the role of specific molecular backbones on the charge transport mechanism, *i.e.*, the transition from tunnelling for short OPI molecules to hopping transport for longer OPI molecules by site-specific disruption of conjugation. For more details concerning this topic, we recommend Luo's review paper[149] that has reported the electrical transport measurement on other long molecules and hopping transport in molecular junctions.

Other intriguing measurements of molecular junctions have recently been reported for functional molecules that consist of both alkyl and conjugated parts.[43,71,129] Nijhuis *et al.* reported a comparison of the rectification ratios of J (at ±1 V) for alkanemonothiol SAMs with ferrocene (Fc) head groups ($SC_{11}Fc$) and without the Fc moiety ($SC_{n-1}CH_3$) using gallium oxide interlayer-based junctions (device structure shown in Fig. 1(h)).[43] The molecular junctions composed of $SC_{11}Fc$ were able to rectify current with large rectification ratios ($|J(-1\ V)|/|J(1\ V)| = 90$–180), whereas the junction lacking the Fc moiety ($SC_{n-1}CH_3$) did not rectify the current nearly as much, exhibiting only minimal rectification ratios (1–5) (Fig. 10(a) and (b)).[43,129] Fig. 10(c) shows the J–V characteristics for Fc-terminated SAM junctions at different temperatures (110, 230, and 293 K). This figure clearly shows that the J values depend on temperature at negative voltages (−0.6 and −1.0 V) (hopping) but are independent of

 This journal is © The Royal Society of Chemistry 2011

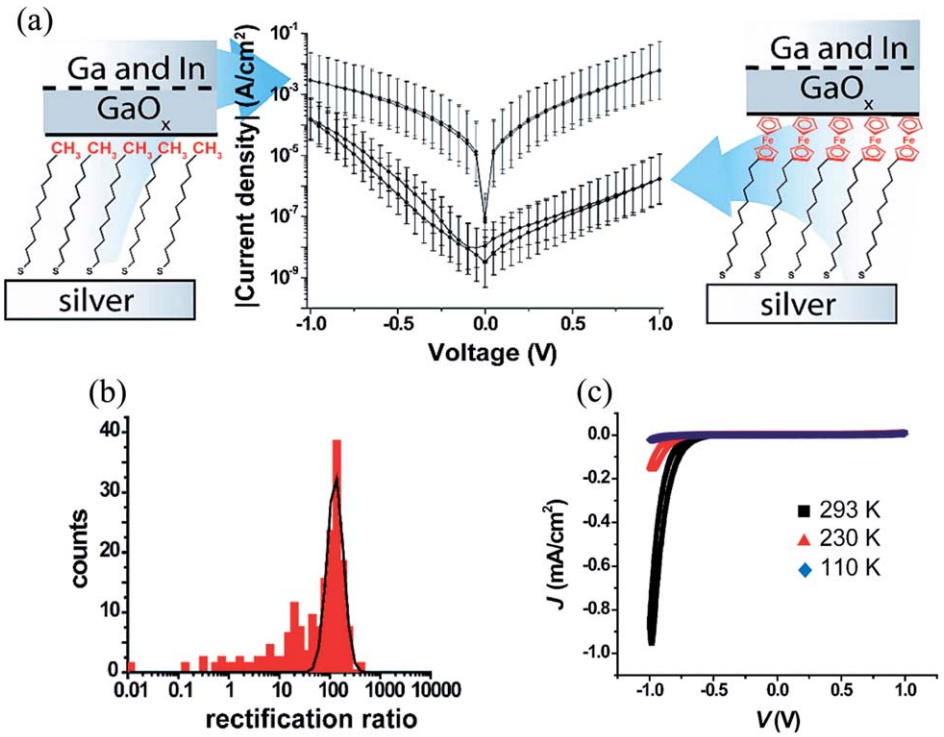

Fig. 10 (a) Schematic showing the gallium oxide (Ga_2O_3)-based molecular junction consisting of (right) $SC_{11}Fc$ and (left) $SC_{10}CH_3$ molecular species. The *J–V* characteristics for $SC_{11}Fc$ and $SC_{10}CH_3$ molecular junctions are shown in the centre. Reprinted with permission from ref. 43, © 2009, American Chemical Society. (b) Histogram of the rectification ratios for $SC_{11}Fc$ molecular junctions with a Gaussian fit. (c) The *J–V* characteristics for $SC_{11}Fc$ molecular junctions measured at different temperatures (110, 250, and 293 K). Reprinted with permission from ref. 129, © 2010, American Chemical Society.

temperature at positive voltages (tunnelling).[129] Based on the temperature-variable *I–V* measurement, these authors suggested that the rectification mechanism across the Fc-terminated SAM junctions may be charge transport processes that change with the bias polarity, *i.e.*, from tunnelling at positive voltages to hopping combined with tunnelling at negative voltages. For molecules, the effect of the detailed locations and quantities of the Fc moiety on the rectification ratio in molecular junctions has also been investigated elsewhere.[135]

Additionally, Lee *et al.* reported a non-volatile memory effect from the molecular monolayer junctions using Ru^{II} terpyridine complexes with thiol-terminated alkyl molecules.[71] Various mono- and di-alkylthiolate-tethered ruthenium(II) terpyridine hexafluorophosphate complexes were designed for the fabrication of molecular memory devices (Fig. 11(a)). Fig. 11(b) shows an example of *I–V* characteristics in a molecular PEDOT:PSS-based device using these SAM molecules. The negative voltage region in Fig. 11(b) shows the reproducible hysteresis (bottom inset of Fig. 11(b)). These authors suggested that the hysteresis is the result of charging/discharging the Ru^{II} terpyridine complexes in the SAM.[71,150] Based on the temperature-independent *I–V* characteristics, the conduction mechanism is a direct tunnelling process that may contain at least a two-step tunnelling process for electron reduction and oxidation through the metal–ligand complex centre.[71,150,151] A write–read–erase–read (WRER) cycle in these molecular junctions was also performed for non-volatile molecular memory phenomena. Fig. 11(c) shows the WRER cycles, which were measured repeatedly for more than 300 cycles.

The electrical properties of the rectifier and memory using the molecular junctions in this section may permit the realisation of more practical molecular device applications.

3.3 Molecular conformation effect

Over the years, several studies have investigated the reversible photo-switch between two different conductance states (ON and OFF) in photochromic molecules.[68,152–159] Among these, diarylethene- and azobenzene-derivative molecules are the most frequently studied candidates for photo-induced switching molecules, based on their conformational changes. Diarylethene-derivative molecules (Fig. 12(a)) have two distinct states, the conjugated (ring-closed) and non-conjugated (ring-open) states of diarylethene, which can be interconverted by exposure to different specific wavelength ranges.[68] The ring-closed form is completed under irradiation in the ultraviolet region (λ = 300–350 nm), and the ring-open form is completed under irradiation in the visible region (λ = 500–600 nm). Fig. 12(a) shows the *J–V* characteristics of the PEDOT:PSS-based junctions, in which the open (OFF) and closed (ON) states of diarylethenes were controlled using irradiation with the above wavelength ranges. The tunnelling current through the closed state in junctions was found to be higher than that through the open state. This is due to the lowering effect of a HOMO–LUMO gap *via* extended π-conjugation (closed state) of a molecule.[68,152,160] Thus, the barrier height for a tunnelling charge in the closed state is expected to be effectively lowered. Furthermore, the photo-switching of this

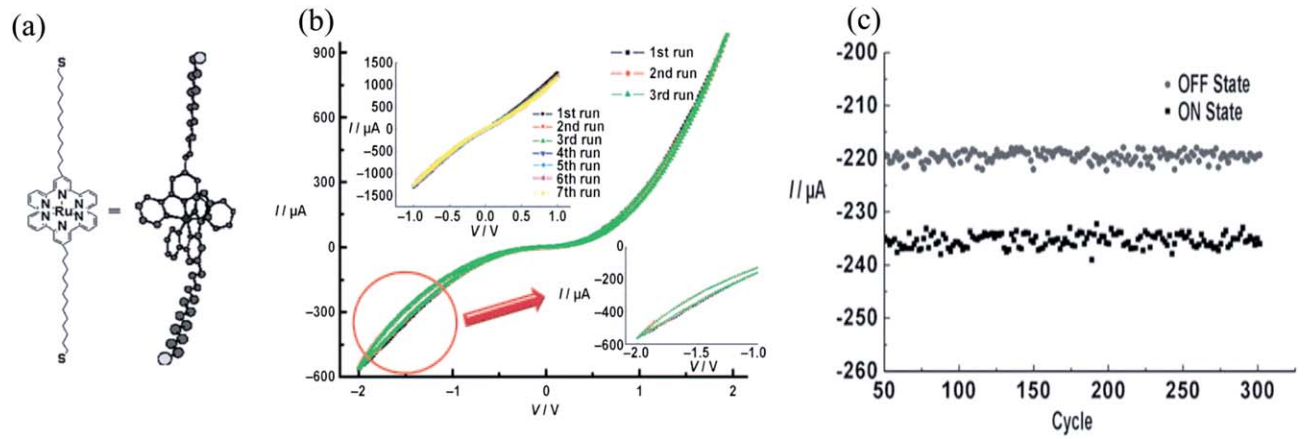

Fig. 11 (a) Example of the ruthenium complex SAMs. (b) Hysteretic *I–V* characteristics for the ruthenium complex SAMs in PEDOT:PSS-based junctions. *I–V* characteristics were recorded by scanning the applied voltage from 0 to +2 V and then to −2 V, followed by a reverse scan from −2 to +2 V. Top inset shows *I–V* characteristics in the junction without ruthenium SAMs. Bottom inset shows the magnification of the *I–V* curve in the hysteretic region. (c) Current in the ON and OFF states as a function of the number of WRER cycles (300 cycles) in the inert condition. Reprinted with permission from ref. 71, © 2009, Wiley-VCH Verlag GmbH & Co. KGaA, Weinheim.

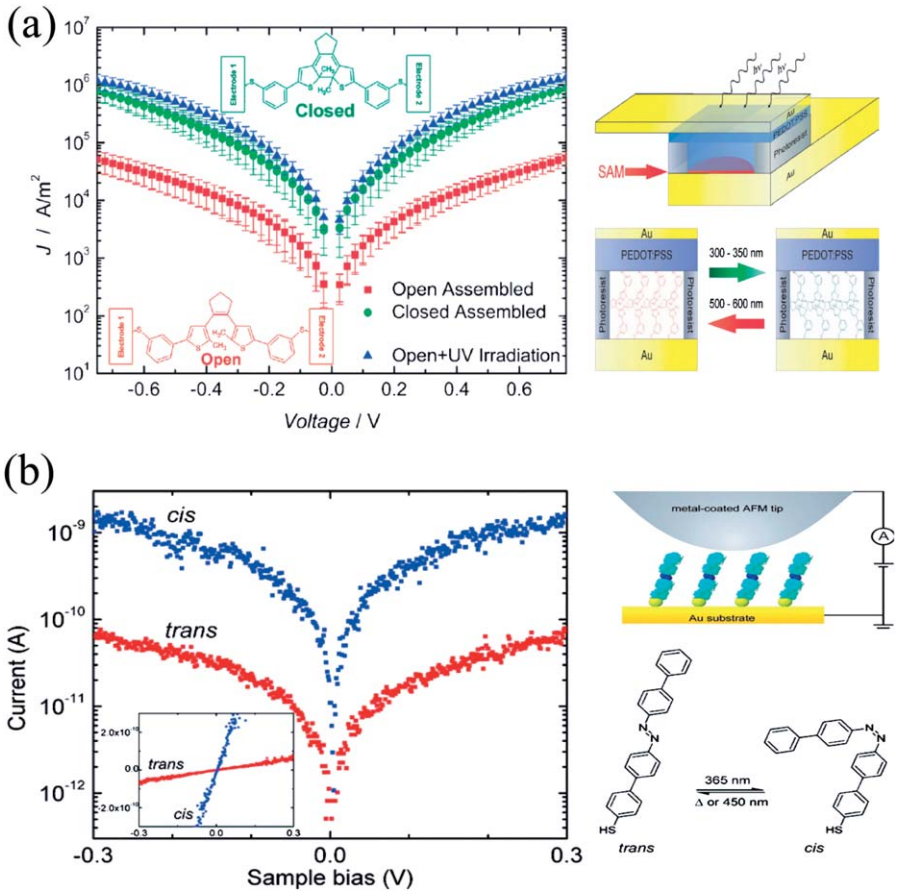

Fig. 12 (a) *J–V* characteristics of the closed (green) and open (red) isomers in the PEDOT:PSS-based molecular junctions, and *J–V* characteristics of the junctions with the open isomer that is self-assembled and subsequently photoisomerised to the closed isomer with UV irradiation (blue). The right side shows a cross-sectional schematic of the PEDOT:PSS-based molecular junction. Using UV (312 nm) illumination, the open, nonconjugated isomer (red) can be converted to the closed, conjugated isomer (green). Visible irradiation of 532 nm reverses the photoisomerisation process. Reprinted with permission from ref. 68, © 2008, Wiley-VCH Verlag GmbH & Co. KGaA, Weinheim. (b) Semilog plot of *I–V* for azobenzene SAMs in CP-AFM junctions, which was recorded before and after UV irradiation and shows larger currents following photoisomerisation into the *cis* conformation (linear scale in inset). Structure of the *trans*- and *cis*-isomers of the light-switchable azobenzene derivatives (bottom right). Reprinted with permission from ref. 156, © 2008, American Chemical Society.

 This journal is © The Royal Society of Chemistry 2011

molecular device was demonstrated from controlled conductance by multiple irradiation sequences.[68] Similarly, azobenzene-derivative molecules can interconvert from *trans*- to *cis*-isomer forms (and *vice versa*) under optical addressing (photo illumination; Fig. 12(b)),[156] which is known as *trans–cis* photoisomerisation.[156,158] The *trans*-isomer is also expected to differ from the *cis*-isomer in conductance as a result of the conformation change.[156–159] Mativetsky *et al.* observed conductance switching associated with the photoisomerisation of azobenzene-based molecules using a CP-AFM approach.[156] Fig. 12(b) shows the I–V curve taken in the linear regime at low voltages (−0.3 to 0.3 V) for *trans*- and *cis*-isomer forms of azobenzene-based molecules. From linear fits of the I–V data, the average resistance of the *trans* state was found to be approximately 30-fold higher than that of the *cis* state. The measured 30-fold decrease in resistance can be explained by the expected decrease in the tunnelling barrier width, resulting from the conformational change of this molecule.

The standing-up and looped formations of long alkanedithiol molecules are also good examples to show the difference in conductance based on a conformational change in a molecule.[161] The formation of the looped phase of alkanedithiol is strongly dependent on the molecular length (particularly when the number of carbons >10) and the number of possible sites for the contact thiols (–S) of molecules to attach to the bottom Au electrode.[161,162] However, the self-assembly process of molecules tends to become more rapid with increasing concentration of molecules,[163,164] which leads to a reduction of the number of possible contact sites for looped formation of alkanedithiols. Therefore, it is possible to form highly looped molecules on substrate particularly when the length of alkanedithiol increases and the concentration of alkanedithiol decreases. Using X-ray photoelectron spectroscopy (XPS) to study the assembled alkanedithiols on an Au film,[161] a low concentration (<0.3 mM) of long alkanedithiols in ethanol was found to lead to a highly looped monolayer. However, a high concentration (>30 mM) led to an almost full standing-up phase on the substrate metal. To determine the influence of the alkanedithiol concentration, the PEDOT:PSS-based molecular devices were fabricated using 0.3 mM, 3 mM, and 30 mM concentrations of DC14 (HS$(CH_2)_{14}$SH) in ethanol solution.[161] Fig. 13 shows the J–V characteristics for DC14 molecular junctions, which were assembled from different concentrations of DC14 in ethanol.[161] The looped molecules were present in the junctions with higher probability because of a decrease in the alkanedithiol concentration in ethanol for the SAM process, resulting in a large increase in conductance and slightly asymmetric J–V characteristics. This is due to a reduction in the tunnelling barrier width and a slight asymmetric contact of looped molecules in the junction structure.

3.4 Transition voltage spectroscopic characteristics

The frontier orbital levels (HOMO energy, E_{HOMO} and LUMO energy, E_{LUMO}) of the molecules, with respect to the Fermi energy level (E_F) of the electrodes, are key factors for determining their electronic charge transport properties.[7,9,165,166] In fact, the difference between the energy levels of the E_{HOMO} or E_{LUMO} from the E_F (*i.e.*, $|E_F - (E_{HOMO}$ or $E_{LUMO})|$) determines the barrier height. A few years ago, Beebe *et al.* found a creative and simple method to estimate the barrier height data in molecular junctions.[56] These authors observed that the molecular junctions formed with π-conjugated thiols having small HOMO–LUMO gaps exhibit a minimum point (transition voltage V_T) on a plot of ln (I/V^2) *versus* $1/V$ that is consistent with a transition from direct tunnelling (DT) to field emission, which is known as Fowler–Nordheim (F–N) tunnelling.[167] Using a transition voltage spectroscopy (TVS) profile from DT to F–N tunnelling, they estimated the position of the nearest molecular orbital levels with respect to the E_F of the electrodes, which can yield information concerning the tunnelling barrier height.

Recently, Araidai and Tsukada investigated the origin of a minimum point appearing in the F–N plot for molecular junctions using two calculation methods, the nonequilibrium Green's-function technique combined with density-functional theory and a tight-binding approximation.[61] Fig. 14 shows the F–N curve corresponding to the integrated $T(E)$ region within the applied voltage window. These authors found that the minimum point in the F–N plot is one of the general features in the integration of the tail of bell-shaped functions, such as the Lorentzian and Gaussian functions. This finding indicates that the minimum point does not necessarily correspond to the transition between the two regimes (DT and F–N tunnelling) and does not necessarily correspond to the voltage of the exact onset of resonant tunnelling. Furthermore, Chen *et al.* reported that the value of $|E_{HOMO} - E_F|/V_T$ (marked as $|\varepsilon_H - E_F|/V_{min}$ in Fig. 15) varies from 0.86 to 2.0, depending on the junction asymmetry; this value is based on extensive *ab initio* calculations of the nonlinear I–V relations for a broad class of molecular junctions.[62] These authors assumed that the position of the transmission function $T(E)$ shifts upward from its original position by a degree of $\eta \times V$ when a finite voltage is applied (Fig. 15 (a)). The parameter η is the asymmetry factor of the coupling. Symmetric coupling corresponds to $\eta = 0$ (in the notation of ref. 62). Therefore, this upward shift of $T(E)$ can lead to a reduction in the V_T (*i.e.*, the $|E_{HOMO} - E_F|/V_T$ value increases) when the electronic coupling is more asymmetric $\eta = 1/2$, as shown in Fig. 15(b). With regard to this finding, the authors emphasised that it is necessary to consider asymmetric coupling for a more comprehensive interpretation of V_T in molecular junctions to fully utilise TVS as a quantitative spectroscopic tool.

The main advantage of the TVS technique is that one can readily obtain the V_T for molecular junctions at relatively low voltages before break-down and without the need for a temperature-variable measurement. In fact, the molecular junctions often become unstable and break down due to the large current density and huge electric field when enough voltage is applied to probe molecular orbital levels.[87,168] For this reason, the TVS technique has become important in the field of molecular electronics.[40,56,73,159,169–171] Now, we will take a close look at the TVS characteristics of molecular junctions in terms of molecular length, structure, contact groups, and conformation.

Fig. 16(a) shows an example F–N plot (ln (I/V^2) *versus* $1/V$) for an Au–anthracenethiol–Au junction using CP-AFM, where the dashed line corresponds to V_T.[56] The shape of the curve in the two bias regions can be predicted within the framework of the conventional tunnelling model (*i.e.*, the Simmons tunnelling model).[172] A plot of ln(I/V^2) *versus* $1/V$ demonstrates the

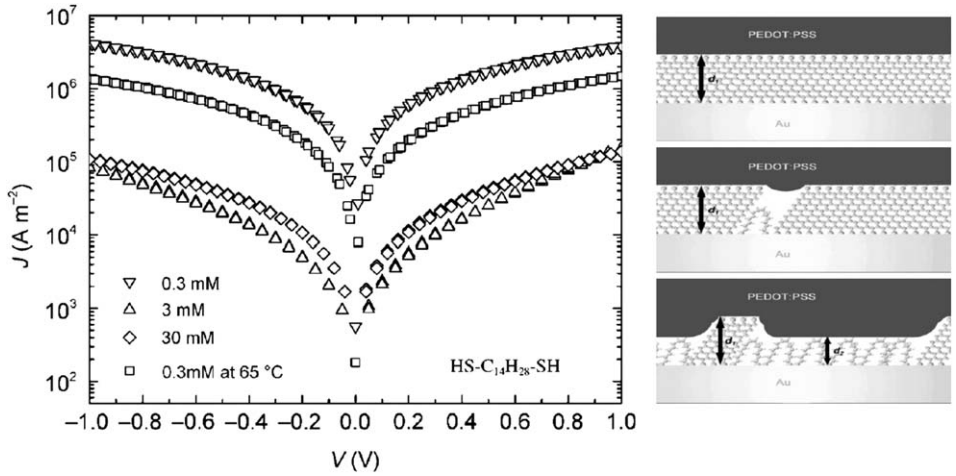

Fig. 13 *J–V* characteristics of PEDOT:PSS-based molecular junctions with DC14 prepared with different concentrations and at different temperatures during the self-assembly process. The almost complete looped phase of the SAM is present after assembly using a 0.3 mM concentration solution, resulting in a 50-fold increase in the current compared with the densely packed and full standing-up phase assembled from a 30 mM concentration solution. The assembly of DC14 at 65 °C results in a decrease of a factor of three at 0.1 V, compared with assembly at room temperature. The right side shows an illustration of the DC14 SAM from different concentrations. (Top: full standing-up phase from a high concentration, centre: low percentage of isolated looping molecules from an intermediate concentration, bottom: dominant looping phase from a low concentration.) Reprinted with permission from ref. 161, © 2008, Wiley-VCH Verlag GmbH & Co. KGaA, Weinheim.

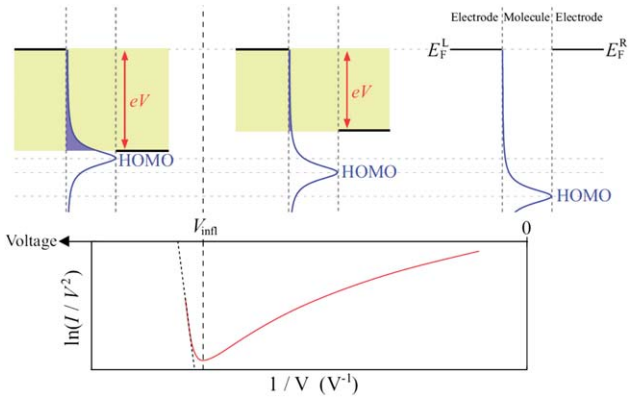

Fig. 14 The scenario for the inflection in the F–N curve. The shaded area indicates the electric current magnitude at V_{infl} (V_T). Reprinted with permission from ref. 61, © 2010, The American Physical Society.

logarithmic growth of the system when the applied bias is less than the barrier height in the DT regime. By contrast, the system exhibits linear decay when the applied bias is higher than the barrier height in the F–N tunnelling regime. The transition from DT to F–N tunnelling accompanies a change in the barrier shape from trapezoidal to triangular and appears as an inflection point (marked as a dashed line) in the plot of ln(I/V^2) *versus* 1/V. The major finding is that the V_T result for the molecular junction shows molecular length-independent or length-dependent properties according to specific molecular structures, such as alkyl (Fig. 16(b)) or π-conjugated molecules (Fig. 16(c)), respectively.[169] In alkanethiol junctions, the TVS results exhibit molecular length-independent transition voltage properties, as shown in Fig. 16(b). This occurs because their HOMO–LUMO gap and $E_F - E_{HOMO}$ offset remain effectively constant as the number of carbon repeat units is changed (*i.e.*, nearly independent of molecular length).[9,109,138] Unlike the alkanethiol

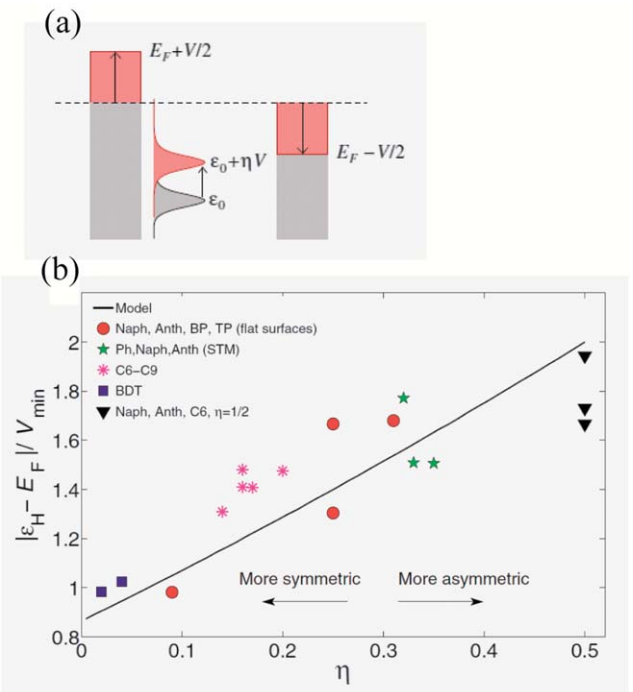

Fig. 15 (a) The schematic illustrates how the molecular level moves under a finite bias voltage. At zero bias, the level is located at 0; however, when a bias voltage is applied, the level tends to follow the chemical potential of the left electrode, due to a stronger coupling to this electrode. (b) A plot of the ratio between the HOMO energy and V_{min} (V_T) *versus* asymmetry parameter (η). The solid line is obtained from a Lorentzian transmission function and symbols are results of *ab initio* finite bias calculations. Reprinted with permission from ref. 62, © 2010, The American Physical Society.

This journal is © The Royal Society of Chemistry 2011

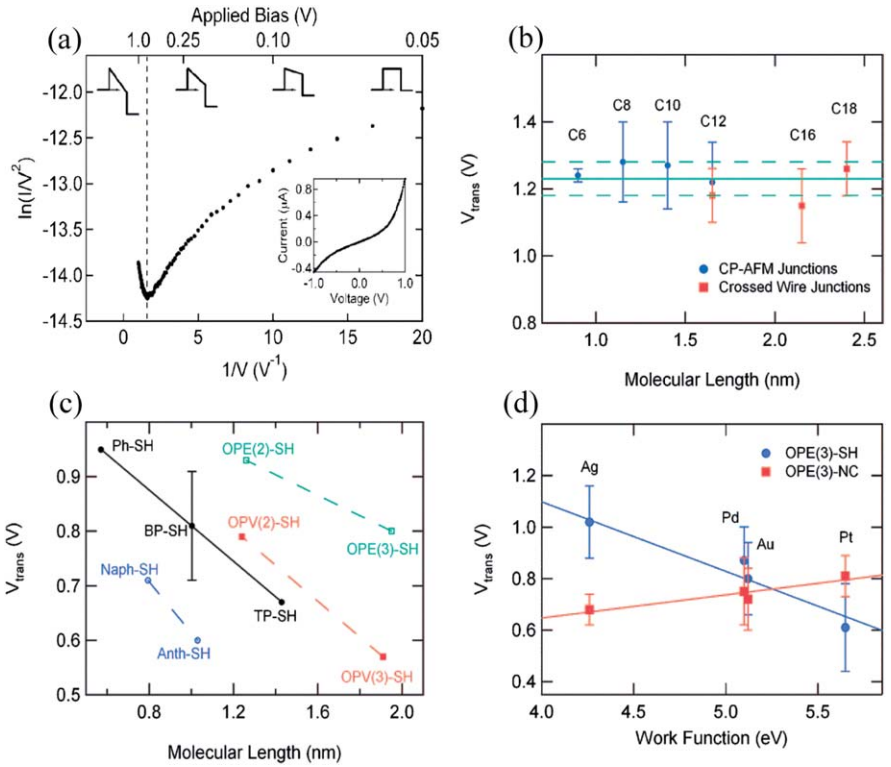

Fig. 16 (a) I–V curves for the Au-anthracenethiol-Au junction measured by CP-AFM. The dashed line corresponds to the transition voltage (V_{trans} or V_T), at which the tunnelling barrier changes from trapezoidal to triangular. The tunnelling barrier shapes are also shown at applied biases. Reprinted with permission from ref. 56, © 2006, The American Physical Society. (b) The V_{trans}–d plot for a series of alkanemonothiols. (c) The V_{trans}–d plot for a series of various π-bonding molecules. (d) V_{trans} as a function of work function for thiol and isocyanide OPE(3) molecules on Ag, Pd, Au, and Pt electrodes. Reprinted with permission from ref. 169, © 2009, American Chemical Society.

junctions, the HOMO levels of π-conjugated molecules (*i.e.*, oligoacene, OPE, or OPV series) are closer to the E_F of the Au electrode when the amount of π-conjugation in these molecules increases (Fig. 16(c)). This approach occurs because the HOMO–LUMO gap for π-conjugated molecules is known to decrease with an increase in conjugation length.[9,48,95] That is, when the amount of conjugation in π-conjugated molecules increases, the V_T position shifts to a lower voltage, as shown in Fig. 16(c).[169] Furthermore, from the measured V_T with various metal electrodes, one can ascertain information concerning dominant tunnelling types, including HOMO-mediated (hole type) *vs.* LUMO-mediated (electron type) tunnelling. These types depend on the E_F position of the metal electrodes with respect to the occupied and unoccupied molecular orbitals. Fig. 16(d) shows the measured V_T as a function of electrode work function (Ag, Pd, Au, and Pt).[169] As the work function of a metal increases, the V_T for OPE(3)–SH decreases, which suggests that HOMO-mediated tunnelling is the dominant channel. By contrast, the V_T for OPE(3)–NC increases as the electrode work function increases, which suggests a LUMO-mediated tunnelling type. The difference in V_T behaviour between OPE(3)–SH and OPE (3)–NC junctions can be explained by the manner in which each functional group influences the energy level alignment when adsorbed onto a metal.[173–175]

The enhancement of field emission transport by molecular tilt configuration in alkyl molecular junctions has been studied, whereby the molecular configuration was varied using a CP-AFM high tip-loading force.[170] In a CP-AFM system, the tip-loading force is directly applied to the molecules to change the junction gap distance by molecular tilt configuration (Fig. 17(a)). Fig. 17(b) shows a plot of ln (I/V^2) *versus* $1/V$ at a fixed tip-loading force of 100 nN for C8, C10, and C12 SAMs. As the molecular length decreases, the minimum point (V_T) occurs at a lower bias, as shown in the inset of Fig. 17(b), because the longer alkanethiol molecules are less tilted under the same tip-loading force. The longer and more rigid alkyl chains, which are stabilised by van der Waals force interactions, can more effectively resist the tip stress.[176,177] The key phenomenon observed in Fig. 17(c) is that the V_T shifts to a lower bias as the tip-loading force increases. This shift occurs because the electric field is enhanced by a reduction in the vertical gap based on molecular tilt configuration, while the tip-loading force is increased. Molecules have been reported to become more tilted with increasing tip-loading force, resulting in a significant contribution of the molecular chain-to-chain transport in the overall conduction within molecular junctions.[170] Thus, the shift of V_T to a lower bias indicates a reduction in the effective barrier height for the molecular junction.

However, recently several theoretical questions about TVS have been raised.[59,61,62,169] For example, the TVS results for certain molecular junctions, such as alkanethiol junctions, exhibit molecular length-independent transition voltage properties (Fig. 16(b)).[169] However, this phenomenon cannot be described within the framework of the conventional model (*i.e.*,

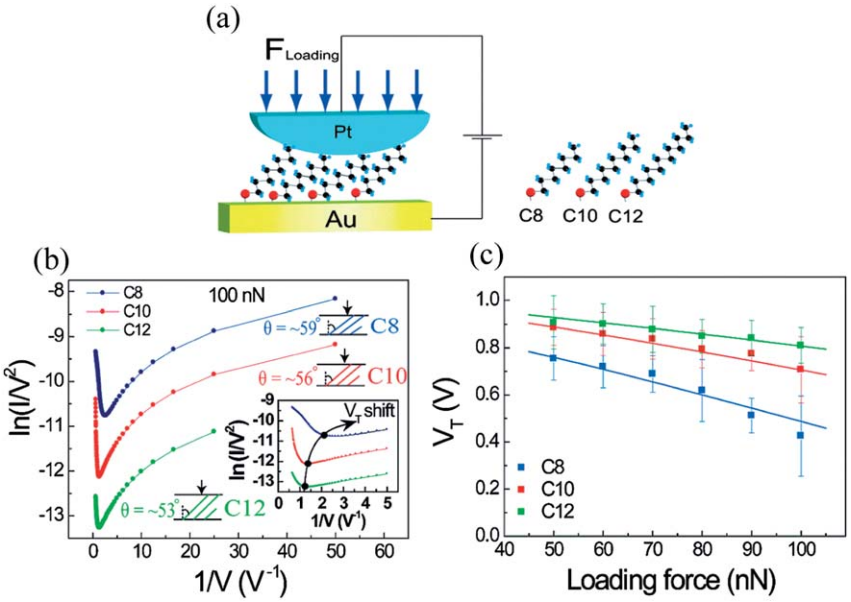

Fig. 17 (a) Schematic of a molecular junction using the CP-AFM method. C8, C10, and C12 molecular structures are shown (right). (b) The plot of ln (I/V^2) *versus* $1/V$ for C8, C10, and C12 at a fixed tip-loading force of 100 nN. Insets show that the transition voltage (V_T) from DT to F–N occurs at a lower bias for shorter molecules. (c) Experimental V_T *versus* tip-loading force for C8, C10, and C12 molecular junctions. Reprinted with permission from ref. 170, © 2009, American Chemical Society.

the Simmons tunnelling model).[172] As shown in Fig. 18(a), remarkably different trends are found between the theoretical and experimental results. The calculated V_T (marked as V_m in Fig. 18) from the rectangular barrier model is not independent of the molecular length, but inversely proportional to it (*i.e.*, $V_T \propto 1/d$). Recently, this disagreement was resolved by Huisman *et al.*, with a coherent molecular model that considered the HOMO level of alkyl molecules with the Lorentzian-based transmission function $T(E)$, which depends explicitly on energy.[59] These authors calculated the *I–V* characteristics for a series of molecular lengths from the Landauer formalism and determined the value of V_T. Fig. 18(b) shows V_m (or V_T) as a function of alkanethiol length d, and the inset shows the corresponding F–N plots. The model theoretically predicted that V_T in alkanethiol molecular junctions was independent of d, except in the case of short molecules (particularly those shorter than ~9 Å). Nevertheless, there was significant discrepancy in the magnitude of V_T between the experimental ($V_T \approx 1.2$ V) and calculated values ($V_T \approx 4.5$ V), as shown in Fig. 16(b) and 18(b). This discrepancy is often ascribed to tunnelling barrier-lowering effects, such as many-electron interactions and image charge.[59,172,178] Many-electron interactions and image charge can lead to a shifting of the $T(E)$ with respect to the E_F of the electrode[178–181] and a narrowing in the width of Lorentzian peaks $T(E_{HOMO\ or\ LUMO})$ under the weak coupling limit.[182,183] Furthermore, the geometric feature of the molecules on the electrodes and their contact sites affect the shape of the transmission function $T(E)$.[178,183,184]

4. Summary and outlook

The advent of molecular electronics has tremendous appeal for scientists and engineers in various research fields because of its novel physical and chemical phenomena as well as its potential technological device applications. The continuous downscaling of device feature size will become scientifically and economically challenging for future integration demands, making molecular-scale control important. As a result, molecular electronics is an active research field of nanotechnology. In this review, various junction platforms were explored for the characterisation of molecular junctions. The major factors that affect intrinsic molecular electronic properties were identified in terms of molecular length, structure, and contact groups. Additionally, we briefly provided the principles of various experimental characterization platforms, including a summary of the electrical characteristics and transport mechanisms for molecular junctions consisting of different molecular components. The goals of this article were to review the current status of research and development regarding these emerging molecular junction platforms and to present recent ideas for device application technologies. In particular, we summarised new device platforms, such as conducting interlayer-based molecular junctions, to promote advanced architectures for high yield and more reliable device applications. As an example, we propose a conceptual device platform that is a cross-point array type structure with graphene-based interlayer molecular electronic devices (Fig. 19). Using this platform, one would be able to measure a large amount of molecular devices with high device yield.

In molecular electronics, the design of standard molecular junctions is a first step for evaluating the characteristics of certain molecular components and understanding their intrinsic electrical properties. Molecular junction design development improves device yield and reproducibility, as well as reducing deviations in intrinsic electrical characteristics. Furthermore, the standard molecular junction design should enable the possibility of massive integration for conventional electronics beyond the simple electrical measurement testbed. It is still necessary to

 This journal is © The Royal Society of Chemistry 2011

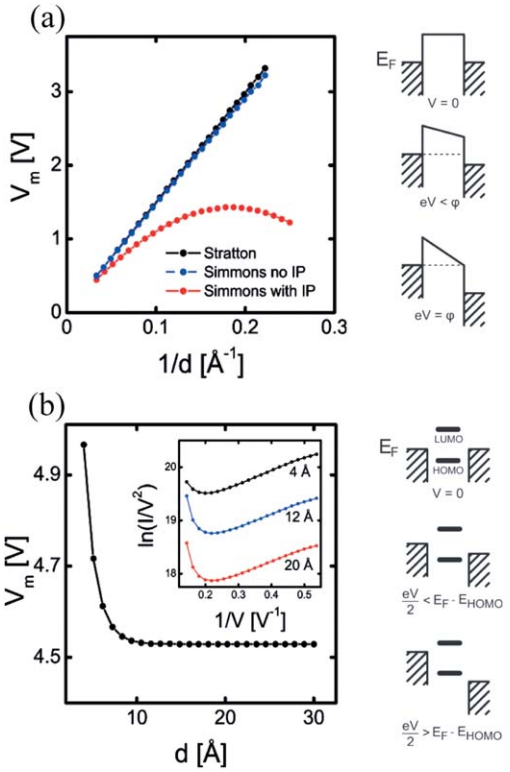

Fig. 18 (a) V_m (V_T) *versus* 1/*d* for a barrier height of 4 eV using various tunnel models (Stratton model; Simmons model without image potential (IP); Simmons model including image potential). V_m (V_T) depends strongly on *d* in all cases. At the right, the Simmons model is shown. Here, a molecule is regarded as a tunnel barrier of height φ and length *d* (top). When a voltage is applied, the barrier is tilted (centre). When eV = φ, the barrier becomes triangular and charges start to tunnel by field emission (bottom). (b) V_m (V_T) *versus* molecular length *d* using a coherent molecular model. At the right, the coherent molecular model is shown. Here, the molecular levels are broadened by interaction with the electrodes (top). When a voltage is applied, the left and right chemical potentials open a window for transport of size (eV) (centre). The current increases dramatically when a level is within the bias window (resonant in tunnelling) (bottom). Reprinted with permission from ref. 59, © 2009, American Chemical Society.

synthesize and to find molecular species to produce robust electronic functionalities, such as switches, diodes, and memory, showing consistent electrical properties across various experimental platforms. These functional molecular components, obtained from a diversity of molecular structures and their energy gaps, should enable self-assembly on electrode surfaces, thermally stable contacts, and functional electronic coupling with electrodes. In addition, identifying and understanding the charge transport mechanism for the control of functional characteristics is an essential component of molecular electronics.

Considerable progress has been made in the advancement of molecular electronics in recent years. However, obstacles still exist in the search for reliable electrical data and standard molecular junction techniques to identify the intrinsic molecular behaviours of molecular devices. Furthermore, a thorough understanding of the charge transport mechanisms for molecular junctions is a substantial issue that must be resolved before any device applications can be realised. From a technical perspective,

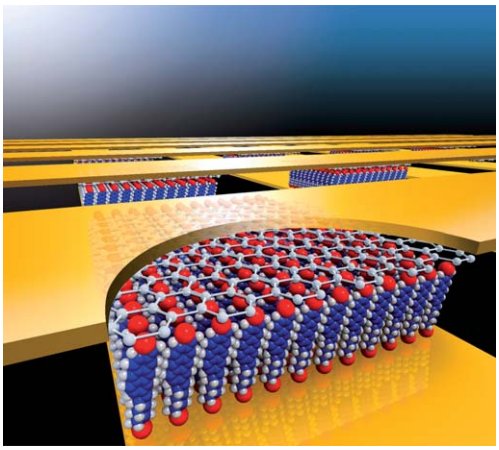

Fig. 19 A conceptual device platform with a cross-point array type structure using graphene-based interlayer molecular electronic devices at high device yield.

it is still tremendously challenging to achieve the ultimate goal of commercial molecular electronic devices. Nevertheless, we believe that the recent growth of experimental and theoretical results will yield feasibility for and insight into the development of molecular electronics in the future.

Acknowledgements

This work was supported by the National Research Laboratory program; a Korean National Core Research Center grant; the World Class University program of the Korean Ministry of Education, Science, and Technology; and the Program for Integrated Molecular Systems at the Gwangju Institute of Science and Technology.

References

1 A. von Hippel, *Science*, 1956, **123**, 315–317.
2 S. W. Herwald and S. J. Angello, *Science*, 1960, **132**, 1127–1133.
3 A. Aviram and M. A. Ratner, *Chem. Phys. Lett.*, 1974, **29**, 277–283.
4 A. Aviram, *Molecular Electronics-Science and Technology*, Am. Inst. of Physics, New York, 1991.
5 R. R. Birge, *Molecular and Biomolecular Electronics*, Am. Chem. Soc., Washington, DC, 1991.
6 A. Ulman, *An Introduction to Ultrathin Organic Films from Langmuir–Blodgett to Self-Assembly*, Academic Press, Boston, CA, 1991.
7 A. Nitzan and M. A. Ratner, *Science*, 2003, **300**, 1384–1389.
8 J. R. Heath and M. A. Ratner, *Phys. Today*, 2003, **56**, 43–49.
9 A. Salomon, D. Cahen, S. Lindsay, J. Tomfohr, V. B. Engelkes and C. D. Frisbie, *Adv. Mater.*, 2003, **15**, 1881–1890.
10 M. A. Reed and T. Lee, *Molecular Nanoelectronics*, American Scientific, Stevenson Ranch, 2003.
11 R. L. McCreery, *Chem. Mater.*, 2004, **16**, 4477–4496.
12 J. C. Love, L. A. Estroff, J. K. Kriebel, R. G. Nuzzo and G. M. Whitesides, *Chem. Rev.*, 2005, **105**, 1103–1170.
13 D. K. Aswal, S. Lenfant, D. Guerin, J. V. Yakhmi and D. Vuillaume, *Anal. Chim. Acta*, 2006, **568**, 84–108.
14 R. Beckman, K. Beverly, A. Boukai, Y. Bunimovich, J. W. Choi, E. DeIonno, J. Green, E. Johnston-Halperin, Y. Luo, B. Sheriff, J. F. Stoddart and J. R. Heath, *Faraday Discuss.*, 2006, **131**, 9–22.
15 B. Ulgut and H. c. D. Abruña, *Chem. Rev.*, 2008, **108**, 2721–2736.
16 J. Zhang, A. M. Kuznetsov, I. G. Medvedev, Q. Chi, T. Albrecht, P. S. Jensen and J. Ulstrup, *Chem. Rev.*, 2008, **108**, 2737–2791.
17 M. Galperin, M. A. Ratner, A. Nitzan and A. Troisi, *Science*, 2008, **319**, 1056–1060.

18 H. Haick and D. Cahen, *Acc. Chem. Res.*, 2008, **41**, 359–366.
19 A. Vilan, O. Yaffe, A. Biller, A. Salomon, A. Kahn and D. Cahen, *Adv. Mater.*, 2009, **20**, 140–159.
20 H. Choi and C. C. M. Mody, *Soc. Stud. Sci.*, 2009, **39**, 11–50.
21 R. L. McCreery and A. J. Bergren, *Adv. Mater.*, 2009, **21**, 4303–4322.
22 L. Tao, H. Wenping and Z. Daoben, *Adv. Mater.*, 2010, **22**, 286–300.
23 J. C. Cuevas and E. Scheer, *Molecular Electronics: An Introduction to Theory and Experiment*, World Scientific Pub. Co. Inc, 2010.
24 M. A. Reed, C. Zhou, C. J. Muller, T. P. Burgin and J. M. Tour, *Science*, 1997, **278**, 252–254.
25 J. Chen, M. A. Reed, A. M. Rawlett and J. M. Tour, *Science*, 1999, **286**, 1550–1552.
26 C. P. Collier, E. W. Wong, M. Belohradský, F. M. Raymo, J. F. Stoddart, P. J. Kuekes, R. S. Williams and J. R. Heath, *Science*, 1999, **285**, 391–394.
27 R. Haag, M. A. Rampi, R. E. Holmlin and G. M. Whitesides, *J. Am. Chem. Soc.*, 1999, **121**, 7895–7906.
28 R. M. Metzger, *Acc. Chem. Res.*, 1999, **32**, 950–957.
29 A. C. Brady, B. Hodder, A. Scott Martin, J. Roy Sambles, C. P. Ewels, R. Jones, P. R. Briddon, A. M. Musa, C. A. Panetta and D. L. Mattern, *J. Mater. Chem.*, 1999, **9**, 2271–2275.
30 W. Liang, M. P. Shores, M. Bockrath, J. R. Long and H. Park, *Nature*, 2002, **417**, 725–729.
31 I. Kratochvilova, M. Kocirik, A. Zambova, J. Mbindyo, T. E. Mallouk and T. S. Mayer, *J. Mater. Chem.*, 2002, **12**, 2927–2930.
32 Y.-L. Loo, D. V. Lang, J. A. Rogers and J. W. P. Hsu, *Nano Lett.*, 2003, **3**, 913–917.
33 D. R. Stewart, D. A. A. Ohlberg, P. A. Beck, Y. Chen, R. S. Williams, J. O. Jeppesen, K. A. Nielsen and J. F. Stoddart, *Nano Lett.*, 2003, **4**, 133–136.
34 B. Xu and N. J. Tao, *Science*, 2003, **301**, 1221–1223.
35 W. Wang, T. Lee, I. Kretzschmar and M. A. Reed, *Nano Lett.*, 2004, **4**, 643–646.
36 L. Venkataraman, J. E. Klare, C. Nuckolls, M. S. Hybertsen and M. L. Steigerwald, *Nature*, 2006, **442**, 904–907.
37 H. B. Akkerman, P. W. M. Blom, D. M. de Leeuw and B. de Boer, *Nature*, 2006, **441**, 69–72.
38 P. Reddy, S.-Y. Jang, R. A. Segalman and A. Majumdar, *Science*, 2007, **315**, 1568–1571.
39 J. E. Green, J. Wook Choi, A. Boukai, Y. Bunimovich, E. Johnston-Halperin, E. DeIonno, Y. Luo, B. A. Sheriff, K. Xu, Y. Shik Shin, H.-R. Tseng, J. F. Stoddart and J. R. Heath, *Nature*, 2007, **445**, 414–417.
40 S. Ho Choi, B. Kim and C. D. Frisbie, *Science*, 2008, **320**, 1482–1486.
41 F. Camacho-Alanis, L. Wu, G. Zangari and N. Swami, *J. Mater. Chem.*, 2008, **18**, 5459–5467.
42 K. Seo, A. V. Konchenko, J. Lee, G. S. Bang and H. Lee, *J. Mater. Chem.*, 2009, **19**, 7617–7624.
43 C. A. Nijhuis, W. F. Reus and G. M. Whitesides, *J. Am. Chem. Soc.*, 2009, **131**, 17814–17827.
44 G. Wang, Y. Kim, M. Choe, T.-W. Kim and T. Lee, *Adv. Mater.*, 2011, **23**, 683.
45 S. Datta, *Electronic Transport in Mesoscopic Systems*, Cambridge University Press, Cambridge, 1995.
46 S. Datta, *Quantum Transport: Atom To Transistor*, Cambridge University Press, Cambridge, 2005.
47 M. D. Ventra, S. T. Pantelides and N. D. Lang, *Phys. Rev. Lett.*, 2000, **84**, 979.
48 S. Hong, R. Reifenberger, W. Tian, S. Datta, J. I. Henderson and C. P. Kubiak, *Superlattices Microstruct.*, 2000, **28**, 289–303.
49 M. P. Samanta, W. Tian, S. Datta, J. I. Henderson and C. P. Kubiak, *Phys. Rev. B: Condens. Matter Mater. Phys.*, 1996, **53**, R7626.
50 A. Nitzan, *Annu. Rev. Phys. Chem.*, 2001, **52**, 681–750.
51 J. M. Seminario, C. E. De La Cruz and P. A. Derosa, *J. Am. Chem. Soc.*, 2001, **123**, 5616–5617.
52 P. E. Kornilovitch, A. M. Bratkovsky and R. Stanley Williams, *Phys. Rev. B: Condens. Matter Mater. Phys.*, 2002, **66**, 165436.
53 J. Taylor, M. Brandbyge and K. Stokbro, *Phys. Rev. Lett.*, 2002, **89**, 138301.
54 M. Paulsson and S. Datta, *Phys. Rev. B: Condens. Matter Mater. Phys.*, 2003, **67**, 241403.
55 G. Wang, T.-W. Kim, H. Lee and T. Lee, *Phys. Rev. B: Condens. Matter Mater. Phys.*, 2007, **76**, 205320.
56 J. M. Beebe, B. Kim, J. W. Gadzuk, C. Daniel Frisbie and J. G. Kushmerick, *Phys. Rev. Lett.*, 2006, **97**, 026801.
57 S. Yeganeh, M. Galperin and M. A. Ratner, *J. Am. Chem. Soc.*, 2007, **129**, 13313–13320.
58 S. S. Datta, D. R. Strachan and A. T. C. Johnson, *Phys. Rev. B: Condens. Matter Mater. Phys.*, 2009, **79**, 205404.
59 E. H. Huisman, C. M. Guédon, B. J. van Wees and S. J. van der Molen, *Nano Lett.*, 2009, **9**, 3909–3913.
60 J. A. Malen, P. Doak, K. Baheti, T. D. Tilley, R. A. Segalman and A. Majumdar, *Nano Lett.*, 2009, **9**, 1164–1169.
61 M. Araidai and M. Tsukada, *Phys. Rev. B: Condens. Matter Mater. Phys.*, 2010, **81**, 235114.
62 J. Chen, T. Markussen and K. S. Thygesen, *Phys. Rev. B: Condens. Matter Mater. Phys.*, 2010, **82**, 121412.
63 J. G. Kushmerick, D. B. Holt, J. C. Yang, J. Naciri, M. H. Moore and R. Shashidhar, *Phys. Rev. Lett.*, 2002, **89**, 086802.
64 M. Elbing, R. Ochs, M. Koentopp, M. Fischer, C. von Hãnisch, F. Weigend, F. Evers, H. B. Weber and M. Mayor, *Proc. Natl. Acad. Sci. U. S. A.*, 2005, **102**, 8815–8820.
65 I. Díez-Pérez, J. Hihath, Y. Lee, L. Yu, L. Adamska, M. A. Kozhushner, I. I. Oleynik and N. Tao, *Nat. Chem.*, 2009, **1**, 635–641.
66 E. Lörtscher, J. W. Ciszek, J. Tour and H. Riel, *Small*, 2006, **2**, 973–977.
67 R. A. Bissell, E. Cordova, A. E. Kaifer and J. F. Stoddart, *Nature*, 1994, **369**, 133–137.
68 A. J. Kronemeijer, H. B. Akkerman, T. Kudernac, B. J. van Wees, B. L. Feringa, P. W. M. Blom and B. de Boer, *Adv. Mater.*, 2008, **20**, 1467–1473.
69 M. A. Reed, J. Chen, A. M. Rawlett, D. W. Price and J. M. Tour, *Appl. Phys. Lett.*, 2001, **78**, 3735–3737.
70 B. Behin-Aein, D. Datta, S. Salahuddin and S. Datta, *Nat. Nanotechnol.*, 2010, **5**, 266–270.
71 J. Lee, H. Chang, S. Kim, G. S. Bang and H. Lee, *Angew. Chem., Int. Ed.*, 2009, **48**, 8501–8504.
72 J. Park, A. N. Pasupathy, J. I. Goldsmith, C. Chang, Y. Yaish, J. R. Petta, M. Rinkoski, J. P. Sethna, H. D. Abruna, P. L. McEuen and D. C. Ralph, *Nature*, 2002, **417**, 722–725.
73 H. Song, Y. Kim, Y. H. Jang, H. Jeong, M. A. Reed and T. Lee, *Nature*, 2009, **462**, 1039–1043.
74 T. D. Dunbar, M. T. Cygan, L. A. Bumm, G. S. McCarty, T. P. Burgin, W. A. Reinerth, L. Jones, J. J. Jackiw, J. M. Tour, P. S. Weiss and D. L. Allara, *J. Phys. Chem. B*, 2000, **104**, 4880–4893.
75 G. Yang and G.-y. Liu, *J. Phys. Chem. B*, 2003, **107**, 8746–8759.
76 P. A. Lewis, C. E. Inman, Y. Yao, J. M. Tour, J. E. Hutchison and P. S. Weiss, *J. Am. Chem. Soc.*, 2004, **126**, 12214–12215.
77 L. Venkataraman, J. E. Klare, I. W. Tam, C. Nuckolls, M. S. Hybertsen and M. L. Steigerwald, *Nano Lett.*, 2006, **6**, 458–462.
78 C. Kergueris, J. P. Bourgoin, S. Palacin, D. Esteve, C. Urbina, M. Magoga and C. Joachim, *Phys. Rev. B: Condens. Matter Mater. Phys.*, 1999, **59**, 12505.
79 J. Reichert, R. Ochs, D. Beckmann, H. B. Weber, M. Mayor and H. v. Löhneysen, *Phys. Rev. Lett.*, 2002, **88**, 176804.
80 R. H. M. Smit, Y. Noat, C. Untiedt, N. D. Lang, M. C. van Hemert and J. M. van Ruitenbeek, *Nature*, 2002, **419**, 906–909.
81 J. G. Kushmerick, D. B. Holt, S. K. Pollack, M. A. Ratner, J. C. Yang, T. L. Schull, J. Naciri, M. H. Moore and R. Shashidhar, *J. Am. Chem. Soc.*, 2002, **124**, 10654–10655.
82 J. G. Kushmerick, J. Naciri, J. C. Yang and R. Shashidhar, *Nano Lett.*, 2003, **3**, 897–900.
83 J. G Kushmerick, C. M. Whitaker, S. K. Pollack, T. L. Schull and R. Shashidhar, *Nanotechnology*, 2004, **15**, S489.
84 K. Slowinski, R. V. Chamberlain, C. J. Miller and M. Majda, *J. Am. Chem. Soc.*, 1997, **119**, 11910–11919.
85 M. A. Rampi, O. J. A. Schueller and G. M. Whitesides, *Appl. Phys. Lett.*, 1998, **72**, 1781–1783.
86 K. Slowinski, H. K. Y. Fong and M. Majda, *J. Am. Chem. Soc.*, 1999, **121**, 7257–7261.
87 R. E. Holmlin, R. Haag, M. L. Chabinyc, R. F. Ismagilov, A. E. Cohen, A. Terfort, M. A. Rampi and G. M. Whitesides, *J. Am. Chem. Soc.*, 2001, **123**, 5075–5085.
88 M. A. Rampi and G. M. Whitesides, *Chem. Phys.*, 2002, **281**, 373–391.

 This journal is © The Royal Society of Chemistry 2011

89 C. Grave, E. Tran, P. Samorì, G. M. Whitesides and M. A. Rampi, *Synth. Met.*, 2004, **147**, 11–18.
90 M. Duati, C. Grave, N. Tcbeborateva, J. Wu, K. Müllen, A. Shaporenko, M. Zharnikov, J. K. Kriebel, G. M. Whitesides and M. A. Rampi, *Adv. Mater.*, 2006, **18**, 329–333.
91 H. Song, M. A. Reed and T. Lee, *Adv. Mater.*, 2011, **23**, 1583–1608.
92 D. J. Wold, R. Haag, M. A. Rampi and C. D. Frisbie, *J. Phys. Chem. B*, 2002, **106**, 2813–2816.
93 J. M. Beebe, V. B. Engelkes, L. L. Miller and C. D. Frisbie, *J. Am. Chem. Soc.*, 2002, **124**, 11268–11269.
94 V. B. Engelkes, J. M. Beebe and C. D. Frisbie, *J. Am. Chem. Soc.*, 2004, **126**, 14287–14296.
95 B. Kim, J. M. Beebe, Y. Jun, X. Y. Zhu and C. D. Frisbie, *J. Am. Chem. Soc.*, 2006, **128**, 4970–4971.
96 X. D. Cui, A. Primak, X. Zarate, J. Tomfohr, O. F. Sankey, A. L. Moore, T. A. Moore, D. Gust, G. Harris and S. M. Lindsay, *Science*, 2001, **294**, 571–574.
97 X. D. Cui, X. Zarate, J. Tomfohr, O. F. Sankey, A. Primak, A. L. Moore, A. L. T. A. Moore, D. Gust, G. Harris and S. M. Lindsay, *Nanotechnology*, 2002, **13**, 5.
98 L. A. Bumm, J. J. Arnold, T. D. Dunbar, D. L. Allara and P. S. Weiss, *J. Phys. Chem. B*, 1999, **103**, 8122–8127.
99 E. A. Weiss, R. C. Chiechi, G. K. Kaufman, J. K. Kriebel, Z. Li, M. Duati, M. A. Rampi and G. M. Whitesides, *J. Am. Chem. Soc.*, 2007, **129**, 4336–4349.
100 V. B. Engelkes, J. M. Beebe and C. D. Frisbie, *J. Phys. Chem. B*, 2005, **109**, 16801–16810.
101 X. D. Cui, A. Primak, X. Zarate, J. Tomfohr, O. F. Sankey, A. L. Moore, T. A. Moore, D. Gust, L. A. Nagahara and S. M. Lindsay, *J. Phys. Chem. B*, 2002, **106**, 8609–8614.
102 T. Morita and S. Lindsay, *J. Am. Chem. Soc.*, 2007, **129**, 7262–7263.
103 J. M. Beebe and J. G. Kushmerick, *Appl. Phys. Lett.*, 2007, **90**, 083117.
104 A. S. Blum, J. G. Kushmerick, S. K. Pollack, J. C. Yang, M. Moore, J. Naciri, R. Shashidhar and B. R. Ratna, *J. Phys. Chem. B*, 2004, **108**, 18124–18128.
105 J. Li and H. D. Abruña, *J. Phys. Chem. B*, 1997, **101**, 2907–2916.
106 J. Li and H. D. Abruña, *J. Phys. Chem. B*, 1997, **101**, 244–252.
107 C. M. Watson, D. J. Dwyer, J. C. Andle, A. E. Bruce and M. R. M. Bruce, *Anal. Chem.*, 1999, **71**, 3181–3186.
108 M. Vasjari, Y. M. Shirshov, A. V. Samoylov and V. M. Mirsky, *J. Electroanal. Chem.*, 2007, **605**, 73–76.
109 W. Wang, T. Lee and M. A. Reed, *Phys. Rev. B: Condens. Matter Mater. Phys.*, 2003, **68**, 035416.
110 W. Wang, T. Lee and M. A. Reed, *Phys. E*, 2003, **19**, 117–125.
111 W. Wang, T. Lee and M. A. Reed, *Rep. Prog. Phys.*, 2005, **68**, 523–544.
112 N. Majumdar, N. Gergel, D. Routenberg, J. C. Bean, L. R. Harriott, B. Li, L. Pu, Y. Yao and J. M. Tour, *J. Vac. Sci. Technol., B: Microelectron. Nanometer Struct.–Process., Meas., Phenom.*, 2005, **23**, 1417–1421.
113 B. de Boer, M. M. Frank, Y. J. Chabal, W. Jiang, E. Garfunkel and Z. Bao, *Langmuir*, 2004, **20**, 1539–1542.
114 H. Haick, J. Ghabboun and D. Cahen, *Appl. Phys. Lett.*, 2005, **86**, 042113.
115 B. C. Haynie, A. V. Walker, T. B. Tighe, D. L. Allara and N. Winograd, *Appl. Surf. Sci.*, 2003, **203/204**, 433–436.
116 C. Zhou, M. R. Deshpande, M. A. Reed, L. Jones Ii and J. M. Tour, *Appl. Phys. Lett.*, 1997, **71**, 611–613.
117 T.-W. Kim, G. Wang, H. Lee and T. Lee, *Nanotechnology*, 2007, **18**, 315204.
118 T.-W. Kim, G. Wang and T. Lee, *IEEE Trans. Nanotechnol.*, 2008, **7**, 140–144.
119 G. Wang, T.-W. Kim, Y. H. Jang and T. Lee, *J. Phys. Chem. C*, 2008, **112**, 13010–13016.
120 G. L. Fisher, A. V. Walker, A. E. Hooper, T. B. Tighe, K. B. Bahnck, H. T. Skriba, M. D. Reinard, B. C. Haynie, R. L. Opila, N. Winograd and D. L. Allara, *J. Am. Chem. Soc.*, 2002, **124**, 5528–5541.
121 A. V. Walker, T. B. Tighe, O. M. Cabarcos, M. D. Reinard, B. C. Haynie, S. Uppili, N. Winograd and D. L. Allara, *J. Am. Chem. Soc.*, 2004, **126**, 3954–3963.
122 H. Haick, O. Niitsoo, J. Ghabboun and D. Cahen, *J. Phys. Chem. C*, 2007, **111**, 2318–2329.
123 A. P. Bonifas and R. L. McCreery, *Nat. Nanotechnol.*, 2010, **5**, 612–617.
124 P. A. Van Hal, E. C. P. Smits, T. C. T. Geuns, H. B. Akkerman, B. C. De Brito, S. Perissinotto, G. Lanzani, A. J. Kronemeijer, V. Geskin, J. Cornil, P. W. M. Blom, B. De Boer and D. M. De Leeuw, *Nat. Nanotechnol.*, 2008, **3**, 749–754.
125 H. B. Akkerman, A. J. Kronemeijer, J. Harkema, P. A. van Hal, E. C. P. Smits, D. M. de Leeuw and P. W. M. Blom, *Org. Electron.*, 2009, **11**, 146–149.
126 S.-I. Na, G. Wang, S.-S. Kim, T.-W. Kim, S.-H. Oh, B.-K. Yu, T. Lee and D.-Y. Kim, *J. Mater. Chem.*, 2009, **19**, 9045–9053.
127 G. Wang, H. Yoo, S.-I. Na, T.-W. Kim, B. Cho, D.-Y. Kim and T. Lee, *Thin Solid Films*, 2009, **518**, 824–828.
128 H. B. Akkerman and B. de Boer, *J. Phys.: Condens. Matter*, 2008, **20**, 013001.
129 C. A. Nijhuis, W. F. Reus, J. R. Barber, M. D. Dickey and G. M. Whitesides, *Nano Lett.*, 2010, **10**, 3611–3619.
130 K. S. Novoselov, A. K. Geim, S. V. Morozov, D. Jiang, Y. Zhang, S. V. Dubonos, I. V. Grigorieva and A. A. Firsov, *Science*, 2004, **306**, 666–669.
131 K. S. Kim, Y. Zhao, H. Jang, S. Y. Lee, J. M. Kim, K. S. Kim, J.-H. Ahn, P. Kim, J.-Y. Choi and B. H. Hong, *Nature*, 2009, **457**, 706–710.
132 G. Jo, M. Choe, C.-Y. Cho, J. H. Kim, W. Park, S. Lee, W.-K. Hong, T.-W. Kim, S.-J. Park, B. H. Hong, Y. H. Kahng and T. Lee, *Nanotechnology*, 2010, **21**, 175201.
133 M. Choe, B. H. Lee, G. Jo, J. Park, W. Park, S. Lee, W.-K. Hong, M.-J. Seong, Y. H. Kahng, K. Lee and T. Lee, *Org. Electron.*, 2010, **11**, 1864–1869.
134 S. Lee, G. Jo, S.-J. Kang, G. Wang, M. Choe, W. Park, D.-Y. Kim, Y. H. Kahng and T. Lee, *Adv. Mater.*, 2011, **23**, 100–105.
135 C. A. Nijhuis, W. F. Reus and G. M. Whitesides, *J. Am. Chem. Soc.*, 2010, **132**, 18386–18401.
136 M. D. Porter, T. B. Bright, D. L. Allara and C. E. D. Chidsey, *J. Am. Chem. Soc.*, 1987, **109**, 3559–3568.
137 C. Vericat, M. E. Vela, G. A. Benitez, J. A. M. Gago, X. Torrelles and R. C. Salvarezza, *J. Phys.: Condens. Matter*, 2006, **18**, R867.
138 J. K. Tomfohr and O. F. Sankey, *Phys. Rev. B: Condens. Matter Mater. Phys.*, 2002, **65**, 245105.
139 E. Lörtscher, H. B. Weber and H. Riel, *Phys. Rev. Lett.*, 2007, **98**, 176807.
140 Y. Hu, Y. Zhu, H. Gao and H. Guo, *Phys. Rev. Lett.*, 2005, **95**, 156803.
141 K. Seo and H. Lee, *ACS Nano*, 2009, **3**, 2469–2476.
142 A. J. Kronemeijer, E. H. Huisman, H. B. Akkerman, A. M. Goossens, I. Katsouras, P. A. van Hal, T. C. T. Geuns, S. J. van der Molen, P. W. M. Blom and D. M. de Leeuw, *Appl. Phys. Lett.*, 2010, **97**, 173302–173303.
143 M. Magoga and C. Joachim, *Phys. Rev. B: Condens. Matter Mater. Phys.*, 1997, **56**, 4722.
144 T. Ishida, W. Mizutani, Y. Aya, H. Ogiso, S. Sasaki and H. Tokumoto, *J. Phys. Chem. B*, 2002, **106**, 5886–5892.
145 S. Wakamatsu, U. Akiba and M. Fujihira, *Jpn. J. Appl. Phys.*, 2002, **41**, 4998–5002.
146 M. Kondo, T. Tada and K. Yoshizawa, *J. Phys. Chem. A*, 2004, **108**, 9143–9149.
147 H. Liu, N. Wang, J. Zhao, Y. Guo, X. Yin, F. Y. C. Boey and H. Zhang, *ChemPhysChem*, 2008, **9**, 1416–1424.
148 R. L. York, P. T. Nguyen and K. Slowinski, *J. Am. Chem. Soc.*, 2003, **125**, 5948–5953.
149 L. Luo, S. H. Choi and C. D. Frisbie, *Chem. Mater.*, 2011, **23**, 631–645.
150 B. Pradhan and S. Das, *Chem. Mater.*, 2008, **20**, 1209–1211.
151 K. Seo, A. V. Konchenko, J. Lee, G. S. Bang and H. Lee, *J. Am. Chem. Soc.*, 2008, **130**, 2553–2559.
152 D. Dulić, S. J. van der Molen, T. Kudernac, H. T. Jonkman, J. J. D. de Jong, T. N. Bowden, J. van Esch, B. L. Feringa and B. J. van Wees, *Phys. Rev. Lett.*, 2003, **91**, 207402.
153 N. Katsonis, T. Kudernac, M. Walko, S. J. van der Molen, B. J. van Wees and B. L. Feringa, *Adv. Mater.*, 2006, **18**, 1397–1400.
154 J. Li, G. Speyer and O. F. Sankey, *Phys. Rev. Lett.*, 2004, **93**, 248302.
155 A. Staykov, D. Nozaki and K. Yoshizawa, *J. Phys. Chem. C*, 2007, **111**, 3517–3521.
156 J. M. Mativetsky, G. Pace, M. Elbing, M. A. Rampi, M. Mayor and P. Samorì, *J. Am. Chem. Soc.*, 2008, **130**, 9192–9193.

157 G. Pace, V. Ferri, C. Grave, M. Elbing, C. von Hänisch, M. Zharnikov, M. Mayor, M. A. Rampi and P. Samorì, *Proc. Natl. Acad. Sci. U. S. A.*, 2007, **104**, 9937–9942.
158 U. Jung, O. Filinova, S. Kuhn, D. Zargarani, C. Bornholdt, R. Herges and O. Magnussen, *Langmuir*, 2010, **26**, 13913–13923.
159 K. Smaali, S. Lenfant, S. Karpe, M. Oçafrain, P. Blanchard, D. Deresmes, S. Godey, A. Rochefort, J. Roncali and D. Vuillaume, *ACS Nano*, 2010, **4**, 2411–2421.
160 J. He, F. Chen, P. A. Liddel, J. Andréasson, S. D. Straight, D. Gust, T. A. Moore, A. L. Moore, J. Li, O. F. Sankey and S. M. Lindsay, *Nanotechnology*, 2005, **16**, 695.
161 H. B. Akkerman, A. J. Kronemeijer, P. A. van Hal, D. M. de Leeuw, P. W. M. Blom and B. de Boer, *Small*, 2008, **4**, 100–104.
162 S. Kohale, S. M. Molina, B. L. Weeks, R. Khare and L. J. Hope-Weeks, *Langmuir*, 2006, **23**, 1258–1263.
163 F. Schreiber, *Prog. Surf. Sci.*, 2000, **65**, 151–257.
164 A. Ulman, *Chem. Rev.*, 1996, **96**, 1533–1554.
165 C. Joachim, J. K. Gimzewski and A. Aviram, *Nature*, 2000, **408**, 541–548.
166 M. Ohara, Y. Kim, S. Yanagisawa, Y. Morikawa and M. Kawai, *Phys. Rev. Lett.*, 2008, **100**, 136104.
167 S. M. Sze and K. K. Ng, *Physics of Semiconductor Devices*, John Wiley & Sons, Inc, New Jersey, 3rd edn, 2007.
168 D. J. Wold and C. D. Frisbie, *J. Am. Chem. Soc.*, 2001, **123**, 5549–5556.
169 J. M. Beebe, B. Kim, C. D. Frisbie and J. G. Kushmerick, *ACS Nano*, 2008, **2**, 827–832.
170 G. Wang, T.-W. Kim, G. Jo and T. Lee, *J. Am. Chem. Soc.*, 2009, **131**, 5980–5985.
171 A. Tan, S. Sadat and P. Reddy, *Appl. Phys. Lett.*, 2010, **96**, 013110–013113.
172 J. G. Simmons, *J. Appl. Phys.*, 1963, **34**, 1793–1803.
173 W. R. Salaneck, K. Seki, A. Kahn and J.-J. Pireaux, *Conjugated Polymer and Molecular Interfaces: Science and Technology for Photonic and Optoelectronic Applications*, Marcel Dekker, New York, 2001.
174 C. D. Zangmeister, S. W. Robey, R. D. van Zee, J. G. Kushmerick, J. Naciri, Y. Yao, J. M. Tour, B. Varughese, B. Xu and J. E. Reutt-Robey, *J. Phys. Chem. B*, 2006, **110**, 17138–17144.
175 C. D. Zangmeister, L. B. Picraux, R. D. van Zee, Y. Yao and J. M. Tour, *Chem. Phys. Lett.*, 2007, **442**, 390–393.
176 X. Xiao, J. Hu, D. H. Charych and M. Salmeron, *Langmuir*, 1996, **12**, 235–237.
177 J. Israelachvili, *Intermolecular and Surface Forces*, Academic Press, New York, 1992.
178 S. Y. Quek, L. Venkataraman, H. J. Choi, S. G. Louie, M. S. Hybertsen and J. B. Neaton, *Nano Lett.*, 2007, **7**, 3477–3482.
179 J. B. Neaton, M. S. Hybertsen and S. G. Louie, *Phys. Rev. Lett.*, 2006, **97**, 216405.
180 P. Darancet, A. Ferretti, D. Mayou and V. Olevano, *Phys. Rev. B: Condens. Matter Mater. Phys.*, 2007, **75**, 075102.
181 M. Koentopp, K. Burke and F. Evers, *Phys. Rev. B: Condens. Matter Mater. Phys.*, 2006, **73**, 121403.
182 A. Ferretti, A. Calzolari, R. Di Felice, F. Manghi, M. J. Caldas, M. B. Nardelli and E. Molinari, *Phys. Rev. Lett.*, 2005, **94**, 116802.
183 K. S. Thygesen and A. Rubio, *Phys. Rev. Lett.*, 2009, **102**, 046802.
184 Z. Li and D. S. Kosov, *Phys. Rev. B: Condens. Matter Mater. Phys.*, 2007, **76**, 035415.

 This journal is © The Royal Society of Chemistry 2011